

**SURFACE STRUCTURE
OF SOME BISMUTH AND ANTIMONY
SINGLE CRYSTAL ELECTRODES**

SILVAR KALLIP

Department of Chemistry, University of Tartu, Estonia
Institute of Physical Chemistry, Chair of Physical Chemistry.

Dissertation is accepted for the commencement of the degree of Doctor of Philosophy in Chemistry on May 4, 2006, by the Doctoral Committee of the Department of Chemistry, University of Tartu.

Doctoral advisor: Prof. Enn Lust, University of Tartu

Opponents: Prof. Fritz Scholz, University of Greifswald
Prof. Emer. Vello Past, University of Tartu

Commencement: June 21, 2006, 2 Jakobi St., room 430

ISSN 1406-0299

ISBN 9949-11-352-0 (trükis)

ISBN 9949-11-353-9 (PDF)

Autoriõigus Silvar Kallip, 2006

Tartu Ülikooli Kirjastus

www.tyk.ee

Tellimus nr. 282

TABLE OF CONTENTS

1. LIST OF ORIGINAL PUBLICATIONS.....	6
2. ABBREVIATIONS USED.....	7
3. INTRODUCTION.....	8
4. LITERATURE OVERVIEW.....	9
4.1. <i>In situ</i> STM.....	9
4.2. The crystallographic properties of Bi and Sb metals.....	12
4.3. <i>In situ</i> study of adsorbed monolayers on single crystal electrodes.....	12
4.4. Roughness calculation.....	14
5. EXPERIMENTAL DETAILS.....	19
6. RESULTS AND DISCUSSION.....	20
6.1. <i>In situ</i> STM measurements.....	20
6.2. Adsorption of camphor on Bi(111) electrode.....	24
6.3. <i>Ex situ</i> SPM measurements and roughness calculations of variously pre-treated Sb surfaces.....	29
6.4. <i>Ex situ</i> AFM measurements and roughness calculations of variously pre-treated Bi surfaces.....	33
7. CONCLUSIONS.....	37
8. REFERENCES.....	39
9. KOKKUVÖTE.....	42
10. ACKNOWLEDGEMENTS.....	44
11. PUBLICATIONS.....	45

1. LIST OF ORIGINAL PUBLICATIONS

- I** **S. Kallip**, P. Laukkanen, A. Jänes, V. Sammelselg, J. Väyrynen, P. Miidla, E. Lust, Investigation of the surface topography and double layer characteristics of variously pre-treated antimony single crystal electrodes, *Surf. Sci.* 532–535 (2003) 1121–1126.
- II** E. Lust, **S. Kallip**, P. Möller, A. Jänes, V. Sammelselg, P. Miidla, M. Väärtnõu and K. Lust, Influence of surface charge density on the electrochemically derived surface roughness of Bi electrodes, *J. Electrochem. Soc.* 150 (2003) E175–E184.
- III** **S. Kallip**, E. Lust, In situ STM studies of Bi(111) electrodes in aqueous electrolyte solutions, *Electrochem. Comm.* 7 (2005) 863–867.
- IV** E. Lust, J. Nerut, E. Härk, **S. Kallip**, V. Grozovski, T. Thomberg, R. Jäger, K. Lust, K. Tähnäs, Electroreduction of Complex Ions at Bismuth and Cadmium Single Crystal Plane Electrodes, *Electrochem. Soc. Trans.* (2006) (accepted).
- V** **S. Kallip**, Heili Kasuk, Vitali Grozovski, Enn Lust, Adsorption of camphor at Bi(111) electrode surface, *Electrochem. Comm.* (submitted).

Author's contribution

Performing all SPM measurements, modelling and interpretation [I–V].
Participated to Roughness calculation and modelling [I,II] and writing the paper [I–V].

2. ABBREVIATIONS USED

AFM	Atomic force microscopy
STM	Scanning tunneling microscopy
UHV-STM	Ultra high vacuum scanning tunneling microscopy
SPM	Scanning probe microscopy
SECM	Scanning electrochemical microscopy
RGRM	random Gaussian roughness model
$\tilde{R}(\kappa, \sigma = 0)$	roughness function (RGRM) at surface charge density $\sigma = 0$
R_{rms}	root mean square roughness
R_{AFM}	geometrical roughness factor
$f_{\text{P-Z}}$	Parsons — Zobel roughness coefficient
EP —	electrochemically polished
CN —	cleaved at the temperature of liquid nitrogen
C —	cleaved at room temperature $T = 298$ K
ECE —	electrochemically etched
C1 —	cut at $T = 298$ K and chemically etched in HNO_3 during 3 sec.
C2 —	cut at $T = 298$ K and chemically etched in HNO_3 during 6 sec.

3. INTRODUCTION

The roughness of the solid electrode surface, describing the real surface structure, is an important parameter in the electrochemistry of solid electrodes as the most of electric double layer and adsorption characteristics are extensive quantities and are referred to the unit apparent (flat cross-section) area of an electrode surface studied [1–8]. Examination of the working area of solid electrodes is a difficult matter owing to the irregularities from micrometer to sub-nanometer level. For that reason the careful microscopic investigations are inevitable. Nowadays the most popular method to apply is scanning probe microscopy (SPM) due to the three-dimensional information available from the measurements.

Sb, Cd and Bi single crystals as very good model electrodes with the stable surface structure in a very wide potential region has been studied at the University of Tartu since 1976. Voluminous database has been collected, containing a lot of information about the influence of the chemical nature and crystallography of electrodes and chemical nature as well as the structure of adsorbing anions or neutral organic compounds on the adsorption parameters.

However, there are no detailed data about the influence of the crystallographic structure of the electrode surface as well as chemical nature of the adsorbing compounds on the kinetics of adsorption of various adsorbates. These data are very important for the development of the modern fuel cells, supercapacitors and highly effective corrosion inhibitors and heterometallic catalysts.

According to obtainable knowledge, there is no data for Bi(111) and Sb(111) planes obtained in the electrochemical *in situ* scanning tunneling microscopy (STM) conditions in literature. Therefore the main aim of these investigations was to develop the experimental conditions needed to obtain the atomic resolution STM data within the wide electrode polarisation region of the Bi(111) and Sb(111) electrode.

The adsorption process of camphor on the electrochemically polished Bi(111)^{EP} plane by using the *in situ* STM method has been studied. For comparison the cyclic voltammetry and impedance methods were applied and the results established were compared with the data obtained for Bi(hkl) [9] and Au(111) in 50 mM Na₂SO₄ + aqueous solutions saturated with camphor [10].

The *ex situ* atomic force microscopy (AFM) and ultra high vacuum scanning tunneling microscopy (UHV-STM) results for variously pre-treated Bi and Sb surfaces has been used as complementary data in terms of the Debye length dependent roughness theory (i.e. non-linear Poisson-Boltzmann theory), recently developed by Daikhin, Kornyshev and Urbakh [1–3].

The experimental roughness function vs. inverse Debye length $\tilde{R}(\kappa, E), \kappa$ – dependencies for the variously treated Bi and Sb electrodes has been composed and compared those results with some calculated $\tilde{R}(\kappa, E), \kappa$ – dependencies.

4. LITERATURE OVERVIEW

4.1. *In situ* STM

The local investigation of electrode surfaces and processes by structure-sensitive probing techniques has become an important topic in electrochemistry, since most practically relevant electrochemical systems are characterized by structural and chemical inhomogeneities of the electrode-electrolyte interface. Such inhomogeneities can influence the local mechanisms of electrochemical reactions in a wide resolution interval extending from the sub-nm scale of surface dislocations and adsorbate layers to structural features in the micrometer range, for example in electrochemical phase formation and dissolution, corrosion, as well as biological membranes and corrosion inhibitor layers [11–23].

The STM uses an atomically sharp probe tip to map contours of the local density of electronic states on the surface. This is accomplished by monitoring quantum transmission of electrons between the tip and substrate while piezoelectric devices raster the tip relative to the substrate. The remarkable vertical resolution of the device arises from the roughly exponential dependence of the electron tunneling process on the tip-substrate separation, d . In the simplest approximation, the tunneling current, I , can be simply written in terms of the local density of states (LDOS; $\rho_s(z, E)$) at the Fermi level ($E=E_F$) of the sample in which V is the bias voltage between the tip and substrate [11–23].

$$I = V\rho_s(0, E_F) \exp(-2\kappa d) \quad (1)$$

and κ is the decay constant, which is related to the magnitude and the shape of the potential barrier. The decay constant may be described by an effective barrier height, φ (eV), according to

$$\kappa = \frac{\pi\sqrt{8m_e\varphi}}{h} \approx 0.51(\varphi(eV))^{1/2} \quad (2)$$

where m_e is a mass of electron.

A value of $\kappa \sim 1\text{\AA}^{-1}$ results in an order of magnitude decrease of the tunneling current per angstrom of electrode separation.

The effective barrier height in electrolyte solution environment is found to be less than that for related vacuum junctions, $0.75\text{\AA}^{-1} \sim 2.15\text{ eV}$ in this instance, (vacuum junction is typically $\sim 1.0\text{\AA}^{-1} \sim 4\text{ eV}$) [11, 12]. The diminished barrier has been associated with tunneling via the " V_0 " level or loosely speaking the "conduction band", of the solvent [13]. Tunneling junctions may also be described in terms of the tunneling conductance, G ,

$$G \approx G_0 \exp(-2\kappa d) \quad (3)$$

where G_0 is associated with quantum-point contact at which the barrier has collapsed ($d = 0$, which corresponds to 2–3 Å internuclear separation) ($G_0 = 1/R_0$, where $R_0 = h/2e^2 = 12.9 \text{ k}\Omega$) [14,22].

The role of solvated ions in the tunneling process has received little attention since these species are unlikely to exist in the junction during atomically resolved imaging. In contrast, ions that are specifically adsorbed on either the tip or substrate will change the LDOS and the surface dipole thereby altering the distribution of the electrostatic potential within the gap in a manner analogous to the vacuum junctions [15, 16]. In cases in which the atomic resonance of an adsorbate lies far above the Fermi level [15], the adsorbate still contributes to the LDOS due to significant broadening of the resonance upon adsorption. If the size of the orbital is such that it extends considerably further out from the surface than the bare substrate wave functions, it will significantly contribute to image formation [15, 17, 18]. For simple anions adsorbed on metal surfaces, it is generally found that the extension of orbitals in space is more important to image formation than the energy of the adsorbate orbitals [17, 18]. However, the recent studies show that image formation in such systems can be highly sensitive to the tunneling conductance.

Well-defined *in situ* STM experiments require the use of a bipotentiostat to independently control the electrochemical potential of the tip and substrate relative to some reference electrode. This configuration is distinct from an UHV experiment in which only the bias between the electrodes needs to be specified. In the electrochemical environment, the tip electrode is simultaneously a tunneling probe and an ultramicroelectrode. Consequently, suitable attention must be given to possible faradic reactions at the tip as suggested in Fig. 1. These reactions may include redox events as well as deposition and dissolution process. Under constant current imaging conditions, the set point current is maintained by a combination of electron tunneling and the faradic process occurring at the tip. Typically, an attempt is made to minimize the faradic contribution at the tip by coating the probe with an insulating substance leaving only the apex of the tip directly exposed to the electrolyte as indicated in Fig. 1. A typical set point current for atomically resolved STM imaging is in the order of ~ 1 to 20 nA. This corresponds to an extremely large current flux $\sim 10^6 \text{ A cm}^{-2}$ between the apex of the tip and substrate area being probed, $< 10^{-14} \text{ cm}^2$. In contrast, any faradic process would be distributed over the exposed area of the tip, which is often in the range of $\sim 10^{-8}$ to 10^{-10} cm^2 such that a 10 nA faradic current would correspond to a current density of 1 to 100 A cm^{-2} . Thus, provided that the tip electrode is suitably coated, a large faradic perturbation is required to destabilize the tunneling-based imaging process. In contrast, the exponential decrease in the tunneling current with increasing tip-substrate separation eventually leads to the limiting case in which $I_{\text{faradic}} \gg I_{\text{tunnel}}$. Under appropriated conditions, the faradic current may be used to form images of the electrochemical reactivity of a surface. This is known as *scanning electro-*

chemical microscopy (SECM) in which the transport and heterogeneous redox activity of species within the junction mediate the tip-substrate interaction [19].

Atomically resolved STM studies require the preparation of a flat surface with well-defined structure [22]. In order to carry out electrochemical studies of solid electrodes, the surface has to be routinely restorable to its original conditions. Flame annealing in a hydrogen oxygen flame has proven to be particularly convenient for rapid refurbishing of the Au(hkl) and Pt(hkl) single crystal surface [5–8,23–32]. It was demonstrated that the crystal quality and surface structure of Au(hkl) and Pt(hkl) electrodes is a very sensitive function of the cooling procedure and slow cooling in an inert gas being preferred over rapid quenching in H₂O for Au(hkl) [5–7,24,26–29]. Electrochemical or chemical polishing (Au, Ag, Cu) [5,24] and electrochemical capillary growth techniques for deposition of single crystals (Ag, Cd) [33,34] may be used as the alternative or additional steps to thermal annealing. The so-called atomic layer deposition from gas phase, as well as electron-beam evaporation and sputtering, provide another avenue for producing flat, highly oriented films [33,35,36].

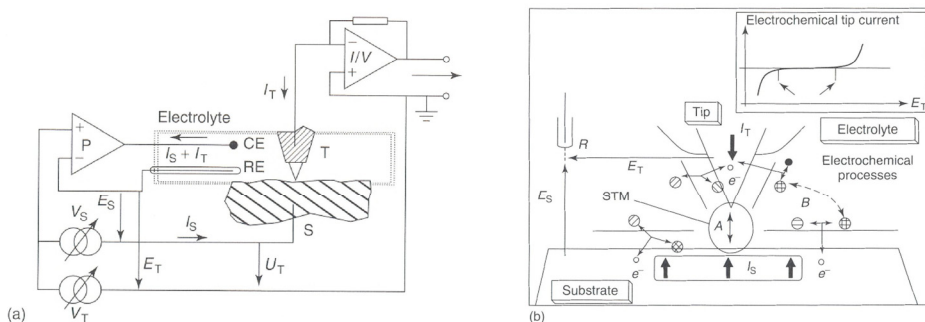


Fig.1. (a) A bipotentiostat allows of the tip (E_T) and substrate (E_S) potential relative to a reference electrode (RE) [20], (b) Schematic presentation of an immersed tunnel junction, at which in addition to direct tunneling between the tip and substrate, there is also the possibility of electrochemical reactions occurring at the tip and substrate. The broken arrow indicates the possibility of linkage between the electrochemical reactions occurring at the tip and substrate, which is the basis of SECM [21].

It was found that the different preparation methods led to the different mesoscopic structures like step bunching that depend on specific preparation procedures used [5–8,22–29,33–40].

The influence of the electrode potential on the surface structure of Au(hkl), Pt(hkl) and Ag(hkl) and other face centred cubic metals has been discussed in many papers [5–8,24–29,37–41]. It was found that the surface structure of Au(hkl) electrodes depends noticeably on the surface charge density and thus,

the zero charge potential and electrochemical work function values depend on the prehistory of the electrode preparation (reconstructed, unreconstructed etc.) and other experimental details [7,24].

4.2. The crystallographic properties of Bi and Sb metals

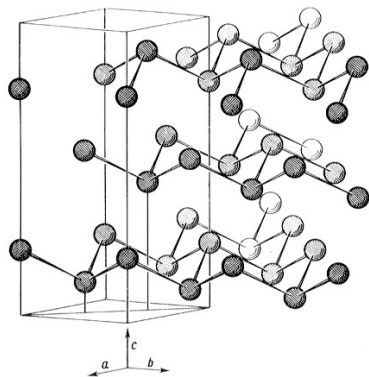


Fig. 2. Layered structure of Bi and Sb crystal [42,43]

Bismuth and antimony has five valence electrons and in its normal crystal modification it is represented by a double layered structure, where each atom has three close neighbours from the same layer (s^2p^3) and three farther neighbours from the second neighbour layer bonds with the aim of hybrid sp^3d^1 orbital, and crystallographic structure can be seen in the figure 2. Bi and Sb crystallises in a rhombohedral Bravais lattice system with an axial angle $\alpha = 57^\circ 14'$.

The distance between atoms inside the same layer is 3.10 Å (Bi) and 2.88 Å (Sb) and the distance between atoms in the neighbouring layers is 3.47 Å (Bi) and 3.38 Å (Sb) [42,43].

Metallic properties of elements of the fifth group depend on the bonding between neighbouring layers and bismuth has the stronger metallic nature than Sb [42,43]. The presence of the covalent semiconductor bonds between the atoms in the Bi and Sb lattice probably fixes the position of the surface atoms more rigidly than in the case of typical metals (Au, Cu, Pt, Pd) [3,5–7,22,24]. According to the previous cyclic voltammetry, impedance and chronocoulometry studies [3,24,44,45], there is no quick surface reconstruction of Sb(hkl) and Bi(hkl) in within the region of ideal polarizability of these electrodes.

It is supposed that the layered structure of Bi and Sb allows to prepare a very smooth atomically flat surface areas as a result of electrochemical polishing procedure used in this work.

4.3. *In situ* study of adsorbed monolayers on single crystal electrodes

Two-dimensional (2D) phase transitions at solid surfaces or in the adsorption adlayers have received much attention in recent years as this phenomenon is related to the very important aspects of surface and materials science connected with the nano- and molecular technology [9,10,39,40,46–54]. The important

characteristics in 2D phase transition are related to the ordered adsorption, island nucleation and growth, oscillating of chemical and electrochemical reactions, surface reconstruction, selective corrosion and corrosion inhibition, chirality of the formed surfaces and electrodeposition mechanism of the metals. It is a very well established fact that the kinetics of 2D condensation is noticeably influenced by the base electrolyte activity and chemical composition [54] as well as adsorption energy of solvent molecules at the surfaces studied (i.e. 2D condensation characteristics depend on the lyophilicity of surfaces investigated). On the other hand, the structure and stability of the adsorbed monolayers are strongly affected by the symmetry of the surface structure of the adsorbate as well as by the adsorbate-adsorbent interaction Gibbs energy and adsorbate-adsorbate, adsorbate-electrolyte, adsorbate-solvent and solvent-solvent lateral interaction energies [9,10,39,40,46–50,53,54]. It is very well demonstrated that the surface structure of Au(hkl) and Pt(hkl) [39,40,46] as well as Ni(hkl) and Cu(hkl) [51,52] is strongly affected by the surface charge density and nature of anions as well as molecular organic compounds adsorbed. At the same time the influence of surface pre-treatment method used for preparation of the Au(hkl), Pt(hkl), Cu(hkl) and Ni(hkl) has crucial importance on the surface structure (reconstructed, unreconstructed etc.) of the electrode used for the *in situ* electrochemistry and ultra-high vacuum surface studies [39,40,46–52].

The exploitation of the classical electrochemical methods (impedance, cyclic voltammetry, chronoamperometry [9,10,50,53,54]) in comparison with the surface sensitive *in situ* techniques such as STM, AFM, second harmonic generation (SHG) and so-called vibrational spectroscopy (SNIFTIR (subtractively normalized interfacial Fourier transform infrared), SEIRAS (surface enhanced infrared reflection absorption spectroscopy), Raman [39,40,46]) methods will provide a complex approximation and strategy to investigate the solid | liquid interfaces in a macroscopic and microscopic (molecular or atomic) levels and to develop in future the general molecular theory taking into account the influence of the crystallographic structure, electronic and chemical nature of the surface as well as the surfactant properties (molecular structure, charge density localisation) on the 2D condensation phenomenon [9,10,39,40,46–54].

According to the Kolb et al. data [54] the shape of cyclic voltammograms and differential capacitance curves depends noticeably on the surface structure of Au(hkl) (Au(111) — thermally reconstructed $\sqrt{3}\times 22$ and 1×1 ; Au(100) — reconstructed 1×1 and hexagonal Structures) studied. However, for all Au surfaces studied, the capacitance pits characteristic of the 2D condensation process has been established in the wide region of surface charge density near zero charge potential. According to the data for the Hg drop electrode [53] the 2D condensation takes place within the wide potential region and the characteristics of the 2D condensation process depend on concentration and nature of the base electrolyte used [53,55,56]. The influence of the surface structure of Bi(hkl) on the thermodynamic characteristics of the camphor adsorption is

comparatively big [9,57]. As these studies at Bi(hkl) have been made during 1977–1980 years [9,57] there is no adsorption kinetics data as well as data at molecular level and new *in situ* STM studies can give more detailed information about the camphor adsorption layer structure on the Bi(111) surface.

4.4. Roughness calculation

The base boundary structure, adsorption properties and electrochemical kinetics of various interfacial charge transfer reactions at the solid surfaces depend significantly not only on the chemical composition but also on the morphology of the surface studied [3–8,23–32,41,44,45,58,59]. Thus, the surface morphology and roughness are important properties as most electrochemical parameters are extensive quantities [3,4]. For the determination of the real surface area of the solid electrodes different *in situ* and *ex situ* methods have been proposed and used [1–4,30,44,45,60–77]. The *in situ* methods more commonly used in electrochemistry to obtain the surface roughness $R = S_{\text{real}}/S_{\text{geom}}$ (where S_{real} and S_{geom} are the real (working) surface and geometrical, so-called flat gross-section surface area, respectively) are: (1) differential capacitance measurements in the region of ideal polarizability [5,8,24,58,60], Parsons–Zobel plot method [63], Valette–Hamelin approach [30] and other similar methods [5,8,24,58,60]; (2) mass transport under diffusion control with assumption of homogeneous current distribution [66]; (3) adsorption of ratio-active organic compounds, hydrogen, oxygen as well as metal monolayers [60,66]; (4) microscopy (optical, electron, STM and AFM) [4,5,8,24,45,60,68–70]; (5) quartz microbalance [70], as well as a number of *ex situ* methods [5,8,24,58,60]. It has to be noted that depending on the irregularity-to-probe size ratio, either the entire surface or only a fraction of it is accessible to a particular measurement. Only when the size of the molecule or ion, used as a probe particle, is smaller than the smallest surface irregularity, the entire surface can be evaluated. It should be noted that each method is applicable to a limited number of electrochemical systems so that a universal method of surface area measurements is not available for the time being. On the other hand, a number of methods used in electrochemistry are not well founded from a physical point of view, and some of them are definitely questionable [24,60]. Thus, it is useful to stress again that the value of R depends on the method used and further more detailed analysis of various methods is indispensable and welcome.

A new roughness theory [1–3] for metal surface with the moderate roughness in the proximity of the zero charge potential, pzc ($E_{\sigma=0}$), has been tested previously for Bi, Sb and Cd electrodes [4,45,73]. In this region of electrode potentials, at the first approximation, the linearized Poisson — Boltzmann approximation seems to be valid, if the mean amplitude of height fluctuations is smaller than the height — height lateral correlation length [1–3]. At these

conditions the effect of surface roughness of the double layer capacitance is determined by an interplay between the Debye length and the scales of roughness, which modifies the Gouy — Chapman result for the diffuse layer capacitance C_{GC} as

$$C = \tilde{R}(\kappa)C_{GC} \quad (4)$$

where C is the differential capacitance and $\tilde{R}(\kappa)$ is the roughness function, which varies between $\tilde{R}(0) = 1$ and $\tilde{R}(\infty) = R > 1$ [1,2]; κ is the Gouy length, *i.e.* the inverse Debye length (κ^{-1}).

According to the Refs [1,2] the experimental roughness function can be expressed as

$$\tilde{R}(\kappa) = \left[\frac{1}{C_{\text{exp}}} - \frac{1}{C_i} \right]^{-1} \cdot \frac{1}{C_{G-C}} \quad (5)$$

where C_i is evaluated from the measurements at high electrolyte concentration according to Valette-Hamelin approach [30]. At the high electrolyte concentrations, when the Debye length κ^{-1} is shorter than the smallest characteristic length of surface inhomogeneity (roughness) l_{min} (*i.e.* $\kappa^{-1} \ll l_{\text{min}}$), the roughness function can be expressed as

$$\tilde{R}(\kappa) \approx R \left\{ 1 - \frac{1}{2R} \frac{\langle H^2 \rangle}{\kappa^2} \right\} \quad (6)$$

where $\langle H^2 \rangle$ is the mean square curvature of surface.

Equation (6) shows that the roughness function $\tilde{R}(\kappa)$ approaches the geometrical roughness factor R at small Debye length κ^{-1} (large concentrations). With the increase of κ^{-1} (the decrease of concentration) it decreases with respect to R , and the correction is proportional to the square of the Debye length, *i.e.* it is inversely proportional to the charge carriers concentration [86,87].

In the range of large Debye lengths (low electrolyte concentrations) the roughness function can be expressed as

$$\tilde{R}(\kappa) \approx 1 + \frac{\kappa h^2}{L} - \kappa^2 h^2 \quad (7)$$

where h is the height of the characteristic size of roughness in the z -direction (h denotes the root mean square departure from medium height); L is the length which is in the order of the maximal correlation length l_{max} (l_{max} is a measure of the average distance between consecutive peaks and valleys on the rough

surface). As expected, at very low electrolyte concentrations ($\kappa^{-1} \rightarrow \infty$; $\kappa^{-1} \gg l_{\max}$) the roughness of surface is not detectable in the capacitance and the first correction to the flat surface result is linear in κ [1,2].

The non-linearized version of new roughness theory, applicable for arbitrary large charges, has been worked out by Daikhin *et al* [3]. Far from $E_{\sigma=0}$ the effects of non-linear screening has been found [3,45], which lead to the dependence of the slope of Parsons — Zobel plots on the electrode charge density, observed experimentally in many works [1–3,5,8,24,30,31,44,45, 58,60,62–65,67,71–77].

It should be noted that the geometrical roughness of the electrode surface usually causes the crystallographic (energetic) inhomogeneity of the electrode studied. Thus, on the surface of polycrystalline electrode there are crystallographically different comparatively homogeneous regions (small single crystal areas) with different zero charge potential $E_{\sigma=0}$ values [24,30,62,64,65,72,73]. This affects the charge distribution along the equipotential surface and thereby the dependence of capacitance on electrolyte concentration, until the characteristic inhomogeneity range is greater than the Debye screening length [1–3,5,8,24,45,58,71–75]. For that reason the crystallographic inhomogeneity causes the dependence of capacitance on the ionic concentration mainly for polycrystals and defect single crystal surfaces where the sizes of homogeneous regions fall in the range between nanometers and about ten of nanometers and can complete with the Debye length (0.98 nm for 0.1 M; and 9.8 nm for 1×10^{-3} M 1–1-electrolyte at $T = 298$ K) and the correlation length of roughness [1–3,5,8,24,45,58,60,71–74].

Using the perturbation — type theory and non-linearized Poisson — Boltzmann theory the apparent surface charge density can be expressed as [3]

$$\sigma = \frac{Q}{S_0} = \frac{e\kappa}{2\pi L_B} \sinh\left(\frac{e\beta E}{2}\right) \times \left\{ 1 + \frac{h^2}{2} \int \frac{d\mathbf{K}}{(2\pi)^2} g(\mathbf{K}) \times K^2 \left[1 - K^2 \left(\kappa \cosh\left(\frac{e\beta E}{2}\right) + q(K) \right)^2 \right] \right\} \quad (8)$$

where Q is the total charge on the metal surface; S_0 is the apparent flat cross-section surface area;

$$L_B = e^2 / \varepsilon k_B T \quad (9)$$

is the Bjerrum length; and $g(\mathbf{K})$ is the height — height correlation function

$$g(\mathbf{K}) \equiv \frac{1}{S_0 h^2} |\xi(\mathbf{K})|^2. \quad (10)$$

In Eq. (8), e is the elementary charge; $\beta = (k_B T)^{-1}$ (T is temperature and k_B is the Boltzmann constant); $\kappa^{-1} = (\varepsilon \beta / 8\pi n e^2)^{1/2}$ is the Debye length (n is the bulk

electrolyte concentration; ε is the dielectric constant of the solvent; E — rational electrode potential (*i.e.* electrode potential vs. zero charge potential); h — the characteristic size of roughness in the z -direction (z -axis pointing toward the electrolyte); \mathbf{K} — the corresponding lateral wave vectors [$\mathbf{K} = (K_x, K_y)$]; $q(K) = \sqrt{\kappa^2 + K^2}$. Differentiation of Eq. (8) over E gives the potential dependent non-linear differential capacitance

$$C = C_{\text{GS}}(E) \tilde{R}(\kappa, E) \quad (11)$$

where C_{GC} is the Gouy — Chapman capacitance for a flat surface.

$$C_{\text{GC}}(E) = \frac{\varepsilon \kappa_{\text{eff}}(E)}{4\pi} \quad (12)$$

with the effective diffuse layer thickness, given by

$$\kappa_{\text{eff}}(E) = \kappa \cosh(e\beta E / 2). \quad (13)$$

$\tilde{R}(\kappa, E)$ is the roughness function, obtained as

$$\begin{aligned} \tilde{R}(\kappa, E) = & 1 + \frac{h^2}{2} \int \frac{d\mathbf{K}}{(2\pi)^2} g(\mathbf{K}) \\ & \times K^2 \left(1 - K^2 \frac{q(K) - \kappa_{\text{eff}}(E) + 2\kappa^2 / \kappa_{\text{eff}}(E)}{(\kappa_{\text{eff}}(E) + q(K))^3} \right). \end{aligned} \quad (14)$$

According to Eq. (14) at $h^2 = 0$, $\tilde{R}(\kappa, E) = 1$ and we shall have the Gouy-Chapman result for the flat surface [1–4,45,60].

Sometimes the apparent surface charge density σ , rather than the electrode potential, is used as an independent electrical variable. At rough surfaces the potential E and the apparent surface charge density σ are related by Eq. (8) and it was found that [3,45]

$$C = C_{\text{GC}}(\sigma) \tilde{R}(\kappa, \sigma) \quad (15)$$

where $C_{\text{GC}}(\sigma)$ at $\sigma = \text{const}$ is given as

$$C_{\text{GC}}(\sigma) = \frac{\varepsilon \tilde{\kappa}_{\text{eff}}(\sigma)}{4\pi} \quad (16)$$

and $\tilde{\kappa}_{\text{eff}}^{-1}(\sigma)$ is the effective thickness of a diffuse layer in terms of σ

$$\tilde{\kappa}_{\text{eff}}^{-1}(\sigma) = \sqrt{\kappa^2 + 4\pi^2 L_{\text{B}}^2 \sigma^2 / e^2}. \quad (17)$$

The roughness function written in terms of κ and σ reads as

$$\begin{aligned} \tilde{R}(\kappa, \sigma) = & 1 + \frac{h^2}{2} \int \frac{d\mathbf{K}}{(2\pi)^2} g(\mathbf{K}) \\ & \times K^2 \left(\left(\kappa / \tilde{\kappa}_{\text{eff}}(\sigma) \right)^2 - \frac{K^2}{\left(\tilde{\kappa}_{\text{eff}}(\sigma) + q(K) \right)^2} \times \left(\left(\kappa / \tilde{\kappa}_{\text{eff}}(\sigma) \right)^2 - 2 \frac{\tilde{\kappa}_{\text{eff}}^2(\sigma) - \kappa^2}{\tilde{\kappa}_{\text{eff}}(\sigma) \left(\tilde{\kappa}_{\text{eff}}(\sigma) + q(K) \right)} \right) \right). \end{aligned} \quad (18)$$

In this work, Eqs. (14) and (18) have been used for the theoretical calculation of the dependence of the roughness function on E and σ , as well as on the scaling parameter κl . Thus, the $\tilde{R}(\kappa, E), \kappa l$ – and $\tilde{R}(\kappa, \sigma), \kappa l$ – dependencies for variously treated Bi electrodes, assuming that the surface roughness is described simply by the one scale correlation function [1–4,45,74], have been calculated.

5. EXPERIMENTAL DETAILS

The surfaces of Bi(111)^C, Sb(111)^C and Sb(001)^C planes have been prepared by cleaving the Bi or Sb single crystals at the temperature of liquid nitrogen in air. In some experiments the cleaved surfaces were additionally chemically etched (Bi(111)^{CE}, Bi(001)^{CE}, Sb(111)^{CE}) with concentrated HNO₃ (during 3 and 6 sec.), electrochemically etched at the surface charge density $i \geq 1.5 \text{ A cm}^{-2}$ (Bi(111)^{ECE}, Sb(111)^{ECE}) or electrochemically polished (Bi(111)^{EP}, Sb(111)^{EP}) in the mixture of KI + HCl + H₂O at current density $i \leq 1.5 \text{ A cm}^{-2}$ [4,44,45].

The Molecular Imaging PicoSPMTM measurement system and the insulated Pt|Ir (70|30) STM tips from Molecular Imaging company have been used for *in situ* STM measurements. In some experiments the used tungsten STM tip has been etched electrochemically using 5M KOH solution and insulated with ApiezonTM wax. The STM-tips and measurement system have been tested and calibrated routinely using the highly oriented pyrolytic graphite cleaved basal plane C(0001)^C (SPITM). All STM images were recorded in constant current mode. The Nanotec Electronica (www.nanotec.es) WSxMTM free software was used for image processing and roughness calculations. The self-made hermetic three-electrode cell with large Pt counter electrode and Ag | AgCl (in the aqueous saturated KCl solution) reference electrode, connected to the *in situ* STM cell through Luggin capillary has been used. The pre-treated (cleaved or electrochemically polished) electrode has been submerged under cathodic polarisation into the aqueous electrolyte solution previously saturated with Ar (92%) + H₂ (8%) mixture. The region of ideal polarizability has been obtained using cyclic voltammetry and a good agreement with the results discussed in various papers [4,24,44,45] has been established.

The water for preparing the solutions was treated with the Milli Q⁺ purification system (resistance > 18.2 MΩ cm). Solutions were prepared volumetrically using Na₂SO₄ purified by triple recrystallization from water, and treated in vacuum to dryness. Na₂SO₄ was calcined at 700 °C immediately prior to the measurements. Compounds studied were extra purified using recrystallization.

The AFM results in air have been obtained in contact mode (CM) regime using with Autoprobe CP (Park SI / Veeco) measurement system with Si₃N₄ MicroleverTM cantilevers.

The UHV-STM studies were carried out by using a Omicron measurement system by pressure 1×10^{-10} torr.

The electrochemical impedance data have been obtained, using Autolab PGSTAT 30 with FRA2 ($\pm 5 \text{ mV}$ modulation) within the frequency region 0.1 to $1 \times 10^5 \text{ Hz}$ and the extrapolated to the condition ac frequency $f \rightarrow 0$ series capacitance values C_s have been used for calculation of Parsons — Zobel plots [63], experimental roughness function, inner layer capacitance and other data discussed [1,4,24,30,44,45].

6. RESULTS AND DISCUSSION

6.1. *In situ* STM measurements

The surface of the cleaved at the temperature of liquid nitrogen $\text{Bi}(111)^{\text{C}}$ consists of atomically smooth terraces with steps of the height of $4.0 \pm 0.2 \text{ \AA}$ (Fig. 3(a)) or of multiple heights [III]. Thus, as can be seen from the Bi crystallographic structure, such a structure is always formed by cleavage occurring between two planes separated by a large distance ($d_2 = 3,47 \text{ \AA}$) [42]. Therefore mainly the van der Waals bonds have been cleaved and the steps have mainly monoatomic height rather than diatomic. The boundaries of triangular shaped terraces are close to the straight lines of the atomic rows on the Bi surface along the [110], [101] and [011] directions (Fig. 3(a)) [42,78]. However, there are some terraces having considerably curved boundaries, and rounded islands of the triangular shape as well as hollows of nanometric dimension, usually of the monoatomic depth. At high magnification, some terrace boundaries show considerable dispersion and can deviate from the direction of atomic rows. Of course the behaviour of the boundaries depends on their direction and the length and thermal motion is the cause for the more extended boundaries being slightly diffused. However, different behaviour of the boundaries can be caused by their various steepnesses on an atomic scale provided by the packing of layers along the [111] direction [42,78].

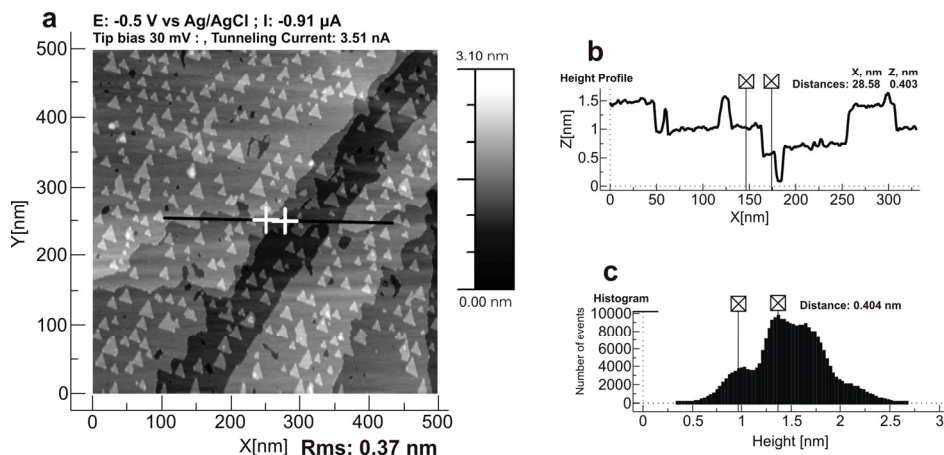


Fig. 3. *in situ* STM image (a), selected surface profile (b) and histogram of the height distribution (c) for the cleaved at the temperature of liquid nitrogen $\text{Bi}(111)^{\text{C}}$ plane in $5 \times 10^{-2} \text{ M Na}_2\text{SO}_4 + 5 \times 10^{-4} \text{ M H}_2\text{SO}_4$ aqueous electrolyte.

In some places the dislocation outcrop can be seen and in some surface regions the very small steps with height lower than the lattice period for Bi have been observed, which are probably caused by the screw dislocations generated during the crystal growth by using the vertical Chohralsky method. These data are in a good agreement with the UHV-STM studies of $\text{Sb}(111)^{\text{C}}$ electrode [1]. The first *in situ* STM studies on $\text{Sb}(111)^{\text{EP}}$ electrode surface show some atomically flat areas and atomic resolution in 5×10^{-2} M $\text{Na}_2\text{SO}_4 + 3.12 \times 10^{-5}$ M H_2SO_4 aqueous solution for $\text{Sb}(111)^{\text{EP}}$ electrode has been achieved similarly to the $\text{Bi}(111)$ electrodes (Fig. 4).

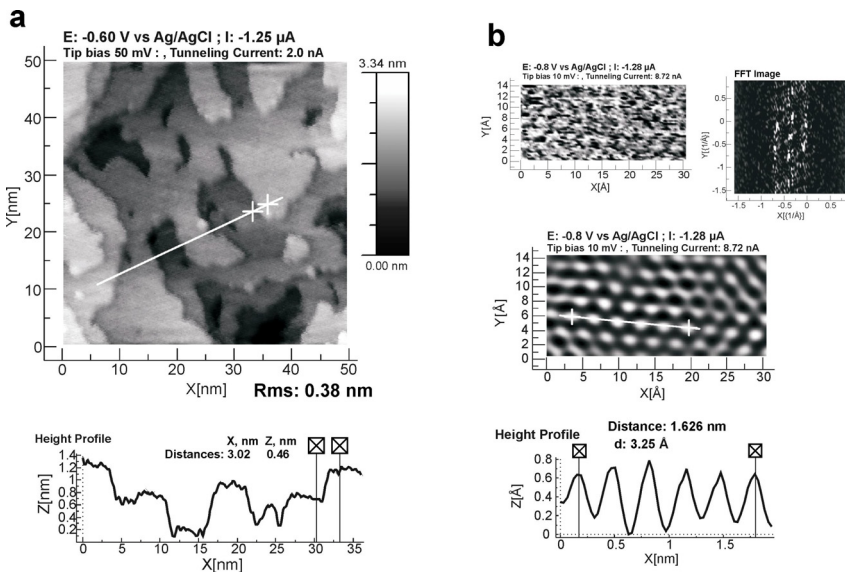


Fig. 4. *in situ* STM image and height profile for $\text{Sb}(111)^{\text{EP}}$ electrode (a) and *in situ* atomic resolution image, FFT (Fast Fourier Transformation) image and calculated periodical signal with surface profile (b) at $E = -0.8\text{V}$ in 5×10^{-2} M $\text{Na}_2\text{SO}_4 + 3.12 \times 10^{-5}$ M H_2SO_4 aqueous solution.

It is very interesting to mention that the position of the two-dimensional crystal, i.e. the nanometric scale triangles (islands as well as hollows) at $\text{Bi}(111)$ surface is very stable during hours under the cathodic polarisation from $-0.7 \leq E \leq -0.1$ V (vs. $\text{Ag}|\text{AgCl}$) as well as under the various potentials applied during hours (Fig. 5(a)) in slightly acidified electrolyte solutions. The root mean square roughness (RMS) vs. cathodic polarisation dependence (Fig. 5(b)) affirmed these data. Thus, in a good agreement with the cyclic voltammetry and impedance data [4,24,44,45,I–V], there are no quick surface reconstruction processes as it has been established for $\text{Au}(\text{hkl})$ [5–7]. At less negative potentials, the surface oxidation and dissolution of the surface occurred and after holding the $\text{Bi}(111)^{\text{C}}$ electrode without polarisation during few minutes, a very complicated surface structure has been observed (Fig. 6).

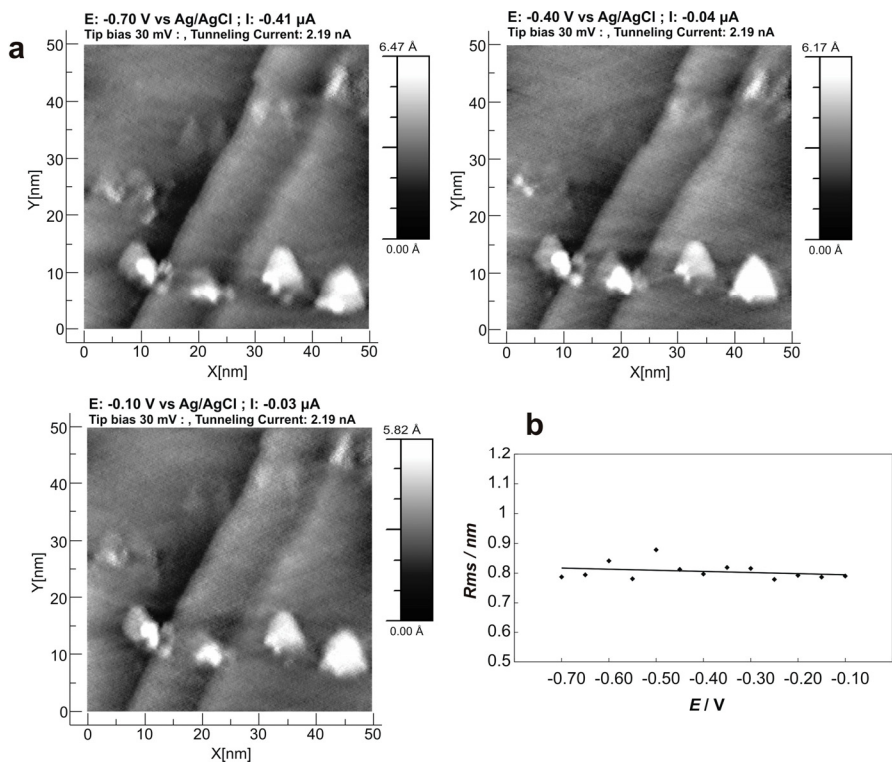


Fig. 5. *in situ* STM images (a) and root mean square roughness (R_{rms}) vs. electrode potential dependence (b) for cleaved $\text{Bi}(111)^{\text{C}}$ plane at various electrode potentials (shown in figure) in $5 \times 10^{-2} \text{ M Na}_2\text{SO}_4 + 5 \times 10^{-4} \text{ M H}_2\text{SO}_4$ aqueous electrolyte.

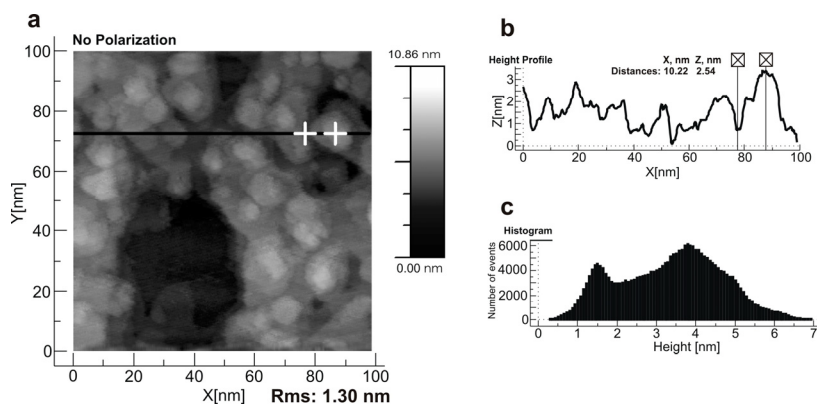


Fig. 6. *in situ* STM image(a), selected surface profile(b) and histogram of the height distribution(c) for the cleaved at the temperature of liquid nitrogen $\text{Bi}(111)^{\text{C}}$ plane in $5 \times 10^{-2} \text{ M Na}_2\text{SO}_4 + 5 \times 10^{-4} \text{ M H}_2\text{SO}_4$ aqueous electrolyte.

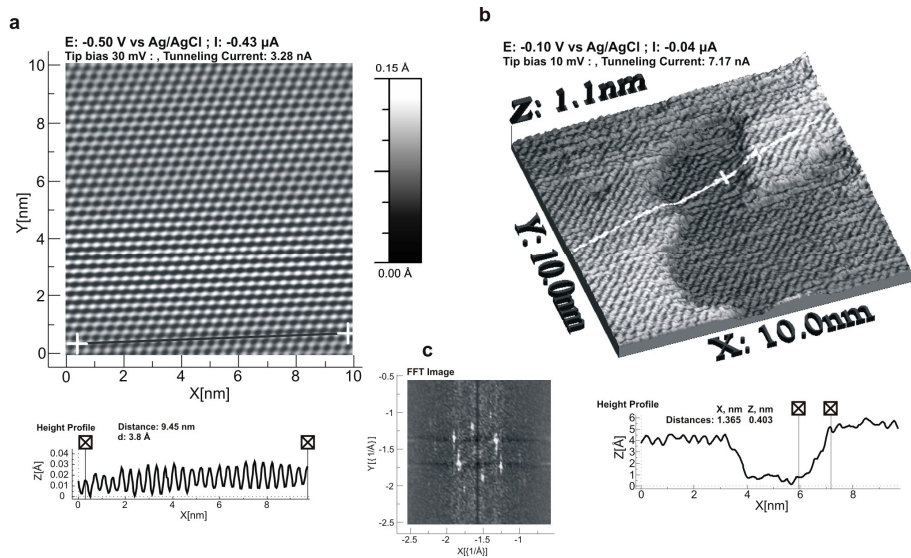


Fig. 7. *in situ* atomic resolution STM images and height profiles for Bi(111)^C electrode at $E = -0.5$ V in 5×10^{-2} M Na₂SO₄ + 5×10^{-4} M H₂SO₄ aqueous solution (a), Bi(111)^{EP} electrode at $E = -0.1$ V in 5×10^{-2} M Na₂SO₄ + 1×10^{-3} M H₂SO₄ aqueous solution (b) and typical FFT image for Bi(111) atomic resolution pictures.

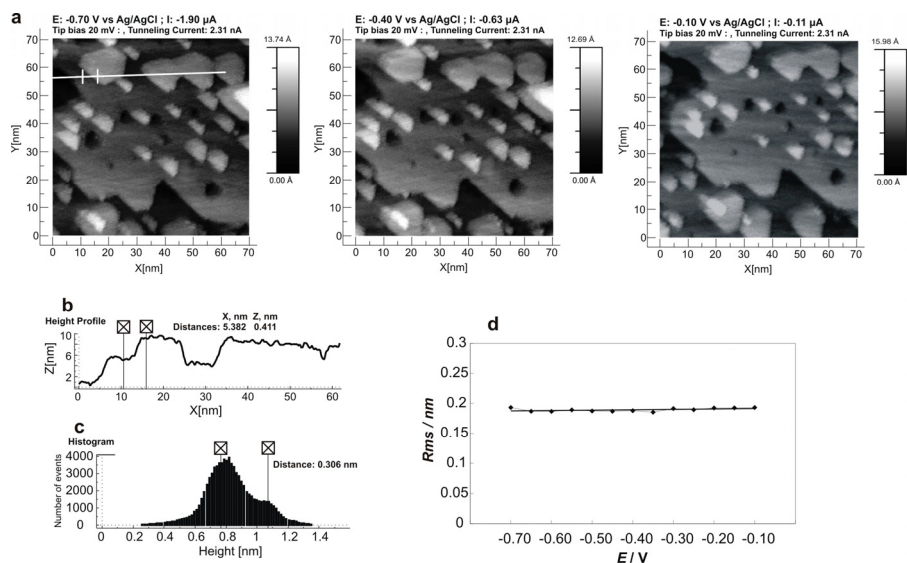


Fig. 8. *in situ* STM images at various electrode potentials (shown in figure) (a), selected surface profile (b), histogram of the height distribution (c) and root mean square roughness (Rms) vs. electrode potential dependence (d) for electrochemically polished Bi(111)^{EP} electrode in 5×10^{-2} M Na₂SO₄ + 5×10^{-4} M H₂SO₄ aqueous solution.

Therefore, usually the potential region from -0.7 to -0.1 V (vs. Ag|AgCl) has been investigated only.

The data in Fig. 7(a) show the atomic resolution picture for the cleaved Bi(111)^C electrode at $E = -0.5$ V. According to these data, the quite regular atomic structure can be observed with interatomic distances $d = 3.8 \pm 0.1$ Å. According to the data in Fig. 7, the triangular structure of atoms prevails at the Bi(111)^C surface.

The data given in Fig. 8(a) shows that the surface of the electrochemically polished Bi(111) is quite smooth and only some monoatomic steps and hollows can be observed. The data in histogram (Fig. 8(c)) and the height profile (Fig. 8(b)) show that there are very wide areas having atomically smooth structure (ca 20...30 nm). However, the very small height fluctuations are possible.

The surface of electrochemically polished Bi(111)^{EP} demonstrates the atomic resolution images (Fig. 7(b)) [IV] like for Bi(111)^C and similarly to the Bi(111)^C electrodes the Bi(111)^{EP} surface is stable under cathodic polarisation from -0.7 to -0.1 V in the 0.05 M Na₂SO₄ + 0.0005 M H₂SO₄ aqueous electrolyte solution and there are no influence of electrode potential on the surface roughness (Fig. 8(d)). Therefore it can be concluded that both Bi(111)^C and Bi(111)^{EP} electrodes can be used for the studies of the more complicated two-dimensional adsorption layers of various organic compounds [V]. It should be noted that differently from Au(hkl) the Bi(111) surface structure does not depend on the surface charge density and potential and within the wide potential region there is no electrode surface restructuring processes caused by the charge density of the metal surface like Au(hkl) [39,40,46]. Thus, the processes prevailing in the 2D adsorption layer of the liquid phase can be studied separately from the surface reconstruction processes, which is characteristic of Au(hkl).

6.2. Adsorption of camphor on Bi(111) electrode

The adsorption process of camphor on the electrochemically polished Bi(111)^{EP} plane by using the *in situ* STM method has been studied [V]. For comparison the cyclic voltammetry and impedance methods were applied and the results established were compared with the data obtained for Bi(hkl) [9] and Au(111) in 50 mM Na₂SO₄ + aqueous solutions saturated with camphor [10].

The cyclic voltammetry and impedance data indicate the formation of the compact (probably 2D condensation or 3D adsorption layer) camphor layer within the wide potential region $-1.25 < E < -0.175$ V (Fig. 9a). Analysis of the Nyquist (Fig. 9b) and Bode phase angle vs. $\log f$ plots [79,80,81] shows that the camphor adsorption is limited mainly by the rate of adsorption step like uracil adsorption on Bi(hkl) [80], with the characteristic relaxation time $\tau_{max} = (2\pi f_{max})^{-1}$ variable from 1.17 sec. (at $E = -1.2$ V) to 0.25 sec. (at $E = -0.65$ V). Differently from the cyclic voltammetry and capacitance data for Au(hkl) | camphor system [10] there is no additional sharp spikes in the I,E - or C,E -

curves for Bi | camphor system, except at very negative and very small negative electrode potentials ($E < -1.35$ and $E \geq -0.15$ V vs. Ag | AgCl), where the desorption of camphor takes place.

However, the *in situ* STM studies indicate the promotion of the detectable (by *in situ* STM method) adsorption adlayer (2D or 3D layer) only at positive surface charge densities ($\sigma > 4 \mu\text{C cm}^{-2}$, $E > -0.45$ V) (Fig. 10, 11) where the simultaneous contact co-adsorption of SO_4^{2-} and camphor takes place with the noticeable partial charge transfer from the SO_4^{2-} anions to the Bi(111) surface atoms [82,83]. The high-resolution images of the high-covered camphor adsorption layer (or 2D layer) at $E > E_{\sigma=0}$ are presented in Fig. 11. A periodic array of bright features is clearly visible at tip bias voltage $E_{\text{bias}} = 93$ mV and at tunnelling current 4.25 nA.

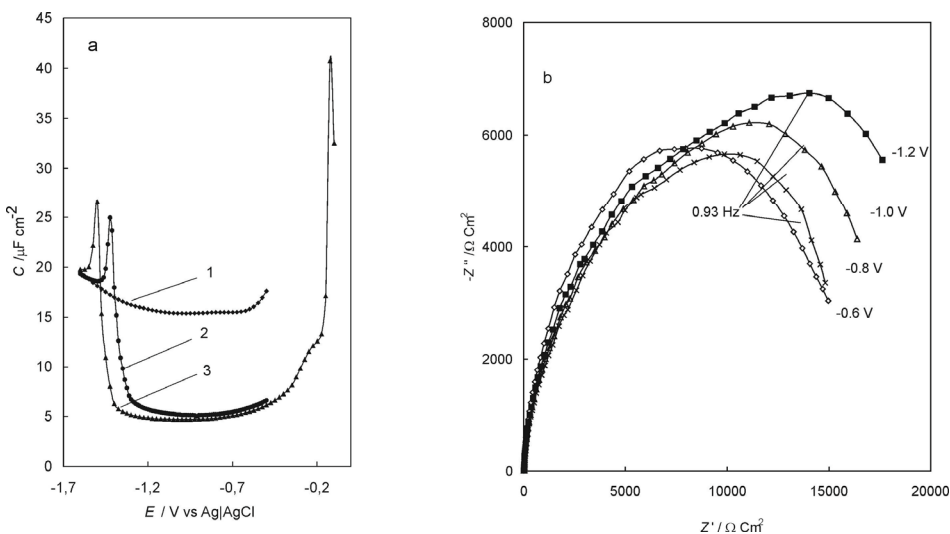


Fig. 9. Differential capacitance C' vs. electrode potential (E) curves (a) for Bi(111) in the base electrolyte (5×10^{-2} M $\text{Na}_2\text{SO}_4 + 2.5 \times 10^{-5}$ M H_2SO_4) (1) and with addition of 5×10^{-3} M (2) and 1×10^{-2} M (3) camphor aqueous solution. Nyquist plots (b) for base electrolyte + 1×10^{-2} M camphor solution at various electrode potential (noted in figure).

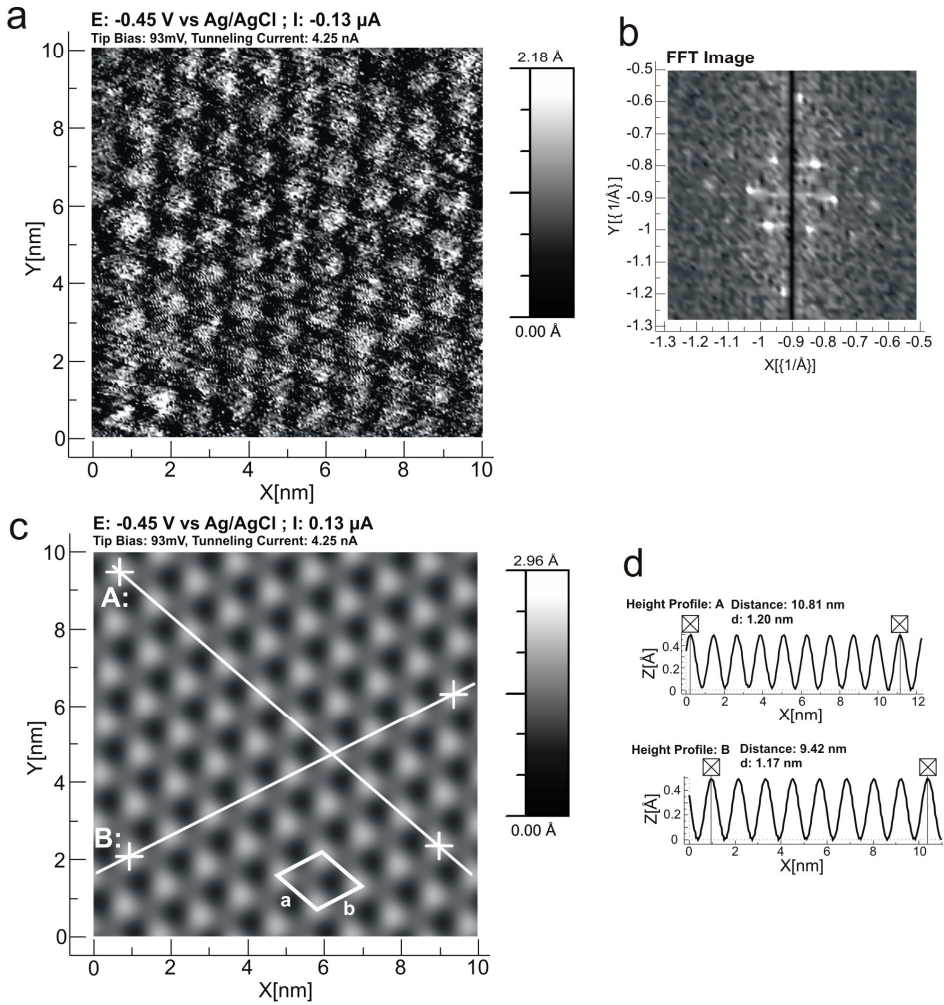
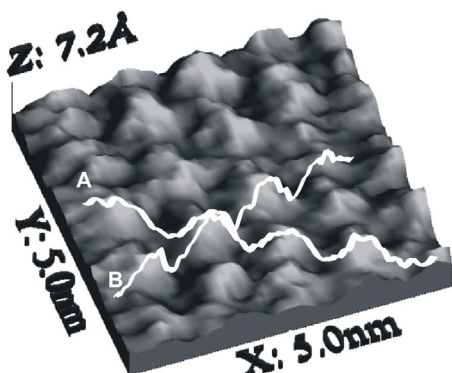


Fig. 10. *in situ* STM image(a), FFT image (b), recalculated periodic signal from FFT (c), selected height profiles (d) of the camphor 2D layer at electrochemically polished Bi(111) electrode in 1×10^{-2} M camphor + 5×10^{-2} M Na_2SO_4 + 2.5×10^{-5} M H_2SO_4 aqueous electrolyte.

a

E: -0.45 V vs Ag/AgCl ; I: -0.09 μ A
 Tip Bias: 89 mV, Tunneling Current: 7.26 nA



b

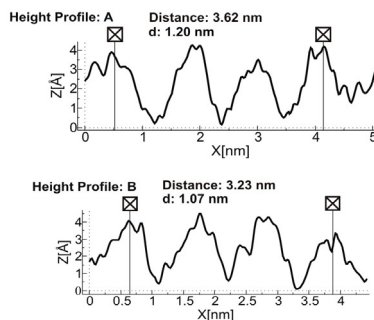


Fig. 11. *in situ* STM image (a), selected height profiles (b) of the camphor 2D layer at electrochemically polished Bi(111) electrode in 1×10^{-2} M camphor + 5×10^{-2} M Na_2SO_4 + 2.5×10^{-5} M H_2SO_4 aqueous electrolyte.

The characteristic dimensions for the nearly rhombohedral structure are $a = 1.20$ nm and $b = 1.17$ nm (Fig. 10). Taking into account the very similar values of a and b , it seems to us that this slightly deformed rhombohedral structure of the adsorption layer with the angles only very slightly differing from $<60^\circ$ and $>120^\circ$ is the more probable structure of the adsorption adlayer. This condition is in good agreement with the rhombohedral Bi crystal unit cell with an axial angle $57^\circ 14'$ and lattice parameter 0.38 nm [42,III]. The first rough estimations of the adsorption layer structure show that the one lattice elementary link (1.20 nm) consists of one co-adsorbed SO_4^{2-} (0.436 nm [84]) and one co-adsorbed camphor molecule and it corresponds to the three Bi lattice cells. The compact adlayer is stable until the onset of camphor desorption from Bi(111) corresponding to the potential of the beginning of oxidation and dissolution of Bi(111) at $E \geq -0.10$ V (vs. Ag|AgCl).

The adlayer dissolves upon a potential excursion toward negative potentials $E < -0.5$ V (Fig. 12) and has not formed in spite holding the Bi(111) electrode at the potential $E_{\text{max}} = -0.65$ V, where the so-called maximum camphor adsorption takes place at the Bi(111) surface according to the data in Fig. 9. At $E = -0.65$ V the atomic resolution picture characteristic of the pure base electrolyte has been observed. This effect can probably be explained by the quite low values of Gibbs adsorption (Γ_{max}), Gibbs adsorption energy (ΔG_A^0) and intermolecular attraction interaction energies $\Delta G_{\text{int}}^0 = -2aRT$ (a is the attraction constant in the Frumkin adsorption isotherm, calculated from impedance data; the data obtained by us are in a good agreement with the results of Refs. [9,57]).

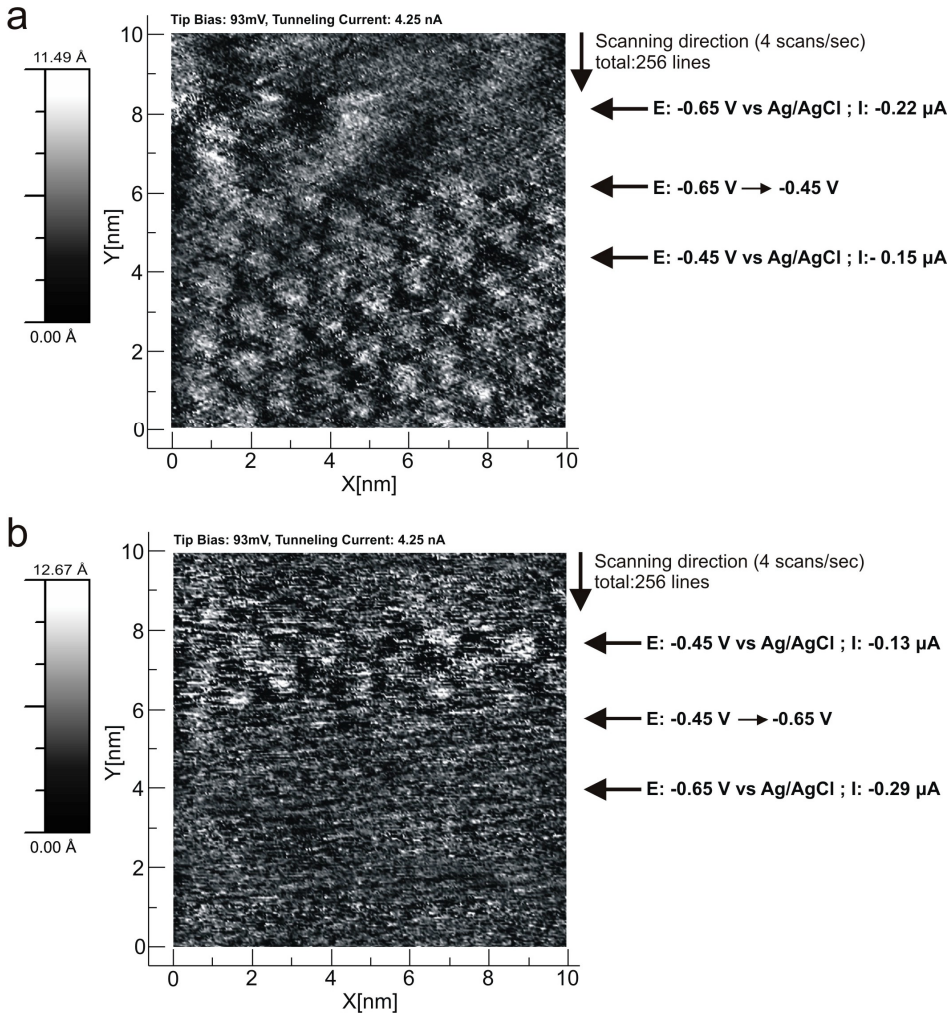


Fig. 12. *in situ* STM images of forming the STM detectable 2D camphor layer by decreasing the cathodic polarization (a) and disappearing the 2D layer by increasing the cathodic polarization (b) at electrochemically polished Bi(111) electrode in 1×10^{-2} M camphor + 5×10^{-2} M Na_2SO_4 + 2.5×10^{-5} M H_2SO_4 aqueous electrolyte.

Differently from the $\text{Au}(111) | 4,4\text{-bipyridine}$ or $2,2$ bipyridine + base electrolyte systems [47,48], where the very high Γ_{max} values have been obtained (Γ_{max} is equal to 6.9×10^{-10} mole cm^{-2} for the most positive adsorption region, 5.7×10^{-10} mole cm^{-2} for the medium adsorption region and 3.4×10^{-10} mole cm^{-2} for the less densely packed layer), the value of Γ_{max} equal to 3.4×10^{-10} mole cm^{-2} for Bi(111) plane indicates the formation of less densely packed adsorption layer, containing a lot of solvent (H_2O) molecules which increase the limiting

capacitance ($C \geq 4,2 \mu\text{F cm}^{-2}$) due to the higher effective dielectric constant value (ϵ_{org}) in comparison with 2D camphor layer at Hg [53,56].

The moderate value of the Gibbs adsorption energy at zero charge potential ($E_{\sigma=0} = -0.63 \text{ V vs. Ag} | \text{AgCl}$) $\Delta G_A^0 = -21.1 \text{ kJ mol}^{-1}$ indicates that there is no noticeable partial charge transfer between camphor and Bi(111) surface atoms, and thus the physical adsorption of camphor takes place, caused mainly by the “squeezing out” effect of the camphor molecules from the base electrolyte solution. Due to the nature of physical adsorption the quite flexible surface structure of the adsorption layer forms and at negative surface charge densities there is no real 2D condensation of camphor at Bi(111) detectable by *in situ* STM method [V].

6.3. *Ex situ* SPM measurements and roughness calculations of variously pre-treated Sb surfaces

The UHV-STM results in Fig. 13 (a) indicate that the surface of Sb(111)^{CN} has a very regular structure and the atomic resolution has been achieved [I]. It should be noted that the correct atomic resolution has been established without any additional treatment of Sb(111)^{CN} surface in UHV. This result indicates that the surface of Sb(111)^{CN} is very inactive and chemically stable in air as well as in the conditions of reduced pressure during many hours.

According to the *ex-situ* AFM results in air (Fig. 13 (b)), the very large atomically flat surface regions ($\sim 1 \mu\text{m}^2$) have been found at Sb(111)^{CN}. In other surface regions the very small steps with height lower than the lattice period of the antimony crystal ($d_1 = 3.37 \text{ \AA}$) have been observed. It should be noted that these small steps are probably connected with the screw dislocations generated during the crystal growth using the horizontal Chohralsky zone refining method.

The *ex-situ* AFM contact mode images (Fig. 14 (b)) show that on the surface of Sb(111)^{CE} (chemically etched during 6 sec in concentrated HNO₃), there are irregular etching pits with the variable depth and width values [I]. According to the data in Fig. 14 (a), there are lot of frequently located and very well oriented small furrows on the big ridges at the surface of cleaved Sb(001)^{CN}. It should be noted that the surface structure of Sb(001)^{CN} (i.e., the profile of the surface in Fig 14(a)) is a quite good example of classical Brownian motion with the Hölder exponent H near to 0.5 [I]. The values of H have been obtained via computing the fractal dimension Δ by the box counting method [85] and then obtaining as $H = 2 - \Delta$. It was found that the size of the boxes did not become less than the minimum of intervals length in numerical investigations. For comparison of the Hölder exponent and $\tilde{R}(\kappa, E)$ values, the systematic studies at the rough electrodes are necessary.

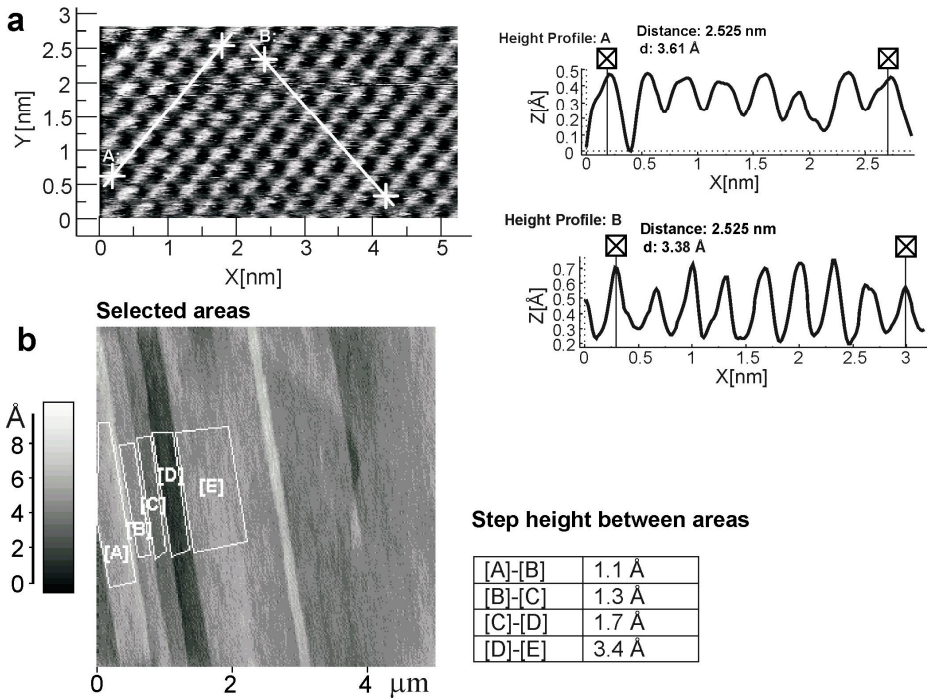


Fig. 13. UHV-STM atomic resolution image and selected surface profile (a) and contact mode AFM image ($5 \times 5 \mu\text{m}$) and results of region height analysis (b) for $\text{Sb}(111)^{\text{CN}}$ surface cleaved at temperature of liquid N_2 .

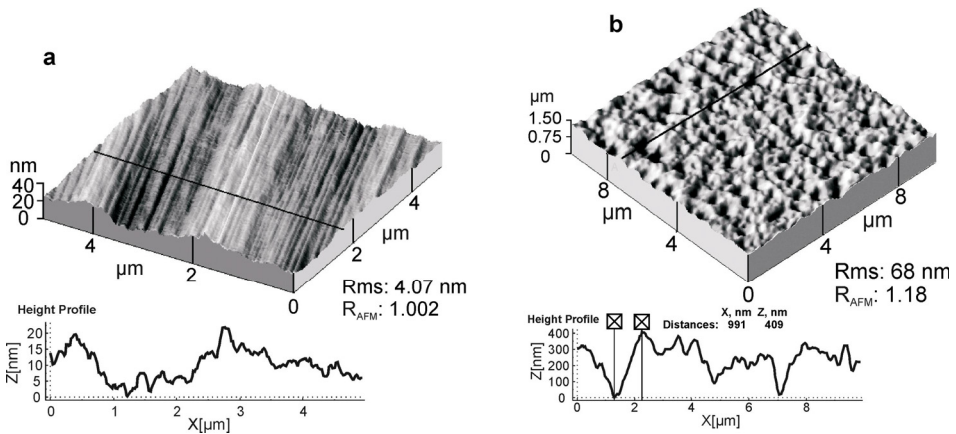


Fig. 14. AFM images and surface profiles for $\text{Sb}(001)^{\text{CN}}$ (cleaved) (a) and $\text{Sb}(111)^{\text{CE}}$ (cleaved and additionally chemically etched surface in HNO_3 during 6 sec.) (b) surfaces.

Table 1. Surface characteristics of variously pre-treated Bi and Sb electrodes.

Electrode	Experimental parameters			RGRM parameters		
	R_{ms} / nm	R_{AFM}	f_{P-Z}	h / nm	l_G / nm	$\tilde{R}(\kappa, \sigma = 0)$
Bi(111) ^{EP}	0.16	1.006	1.03	0.3	100	1.02
Bi(111) ^{CN}	0.36	1.009	1.03	0.5	15	1.10
Bi(111) ^C	0.44	1.01	1.06	0.5	10	1.15
Bi(111) ^{ECE}	13.6	1.25	1.18	0.5...1.0	1.0...3.0	1.35
Bi(001) ^{C1}	118	1.13	1.23	5	10	1.60
Bi(111) ^{C1}	348	1.07	1.26	10	20	1.80
Bi(001) ^{C2}	532	1.30	1.38	15	20	2.05
Sb(111) ^{CN}	0.11	1.0001	1.03	0.6	50	1.03
Sb(111) ^{EP}	0.10	1.0001	1.05	0.6	40	1.03
Sb(111) ^{ECE}	0.18	1.09	1.13	1.5	5.0	1.22
Sb(111) ^{CE}	68	1.18	1.21	3.0	20	2.5
Sb(001) ^{CN}	4.07	1.002	1.28	5.0	10	2.5

^{EP} — electrochemically polished

^{CN} — cleaved at the temperature of liquid nitrogen

^C — cut at room temperature $T = 298$ K

^{ECE} — electrochemically etched

^{C1} — cut at $T = 298$ K and chemically etched in HNO_3 during 3 sec.

^{C2} — cut at $T = 298$ K and chemically etched in HNO_3 during 6 sec.

R_{ms} — root mean square roughness (from AFM data)

R_{AFM} — geometrical roughness factor (from AFM data)

RGRM — random Gaussian roughness model

f_{P-Z} — Parsons — Zobel roughness coefficient (obtained from impedance data)[60]

h — root mean square height of surface roughness (fitting parameter in RGRM)

l_G — characteristic lateral correlation length (fitting parameter in RGRM)

$\tilde{R}(\kappa, \sigma = 0)$ — roughness function at surface charge density $\sigma = 0$.

For the characterisation of variously pre-treated Sb(111)^{CN} electrodes, the root mean square roughness (R_{ms}) and the so-called surface roughness factor values $R_{AFM} = S_{AFM} / S_{geom}$ (S_{AFM} is the surface area obtained from AFM images and S_{geom} is the flat gross-section area) have been calculated and are given in Table 1. In this table the electrochemical (effective) values of surface roughness, obtained using classical Parsons — Zobel and Valette — Hamelin approaches (f_{P-Z}) [30,63] are given too.

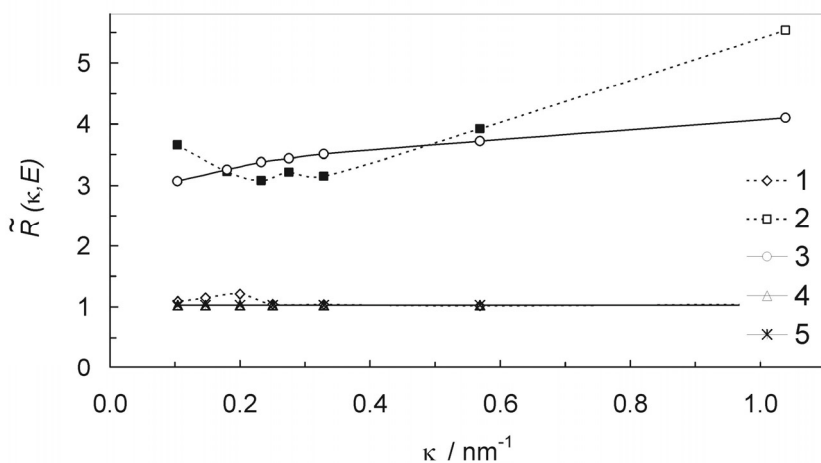


Fig. 15. Experimental roughness function vs. inverse Debye length plots for $\text{Sb}(111)^{\text{CN}}$ (1) and $\text{Sb}(001)^{\text{CN}}$ (2) and calculated ones, using random Gaussian roughness model (RGR) at $h = 5.0 \text{ nm}$ and $l = 10.0 \text{ nm}$ (3), and at $h = 0.6 \text{ nm}$ and $l = 50.0 \text{ nm}$ (4,5) for various rational potentials (V vs. $E_{\sigma=0}$): 0.0 (1–4) and 0.15 (5).

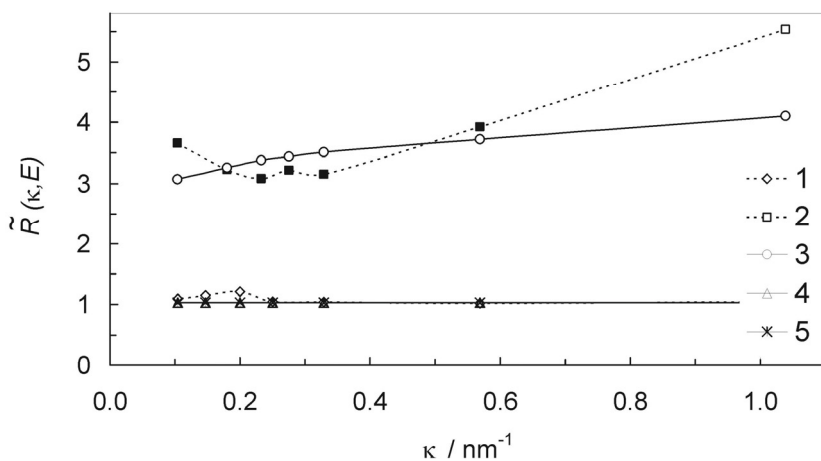


Fig. 16. Experimental roughness function vs. inverse Debye length plots for $\text{Sb}(111)^{\text{CE}}$ (1) and $\text{Sb}(111)^{\text{ECE}}$ (2) and calculated ones (according to RGR model) at $h = 3.0 \text{ nm}$ and $l = 20 \text{ nm}$ (3,4), and at $h = 1.5 \text{ nm}$ and $l = 5.0 \text{ nm}$ (5,6) at E (V): 0.0 (1–3,5) and 0.15 (4,6).

Comparison of *ex-situ* and electrochemical parameters shows that the effective electrochemical roughness values for $\text{Sb}(111)^{\text{CN}}$ and electropolished $\text{Sb}(111)^{\text{EP}}$

are noticeably higher than the R_{AFM} values. This is probably mainly caused by the fact that there are some deviations from the Gouy — Chapman diffuse layer theory because the value of f_{p-z} , higher than unity has been established for the energetically homogeneous Hg-electrode ($f_{p-z} = 1.06 \dots 1.07$) as well [31].

The data in figures 15 and 16 indicate that the roughness function obtained from impedance data (from series capacitance C_s values at $f = 0$ Hz) increases in the order $Sb(111)^{CN} < Sb(111)^{EP} < Sb(111)^{ECE} < Sb(111)^{CE} < Sb(001)^{CN}$, thus, in the same order as it was found using the UHV-STM and AFM data. The very high $\tilde{R}(\kappa, E)$ values for $Sb(001)^{CN}$ are determined by the good correlation of the dimensions of solvated ions and the medium height of the frequently located “furrows” on the surface of big “ridges” (Fig. 14 (b)) (i.e. the height of the small ridges (2–20 nm)) is of the same order as the Debye screening length for 0.1 M and 0.001 M NaF aqueous solutions (0.98 and 9.8 nm, accordingly). According to the results of calculations the influence of the surface defects, higher than 10 nm, on the $\tilde{R}(\kappa, E)$ values is very weak for the electrolytes with concentration higher than 0.001 M.

As it can be seen in Figs. 15 and 16, as for rough Bi and Cd [4,30] electrodes, in the region of moderate electrolyte concentrations, there is a good agreement between experimental and calculated $\tilde{R}(\kappa, E)$ -function values [I]. The noticeable deviation of experimental $\tilde{R}(\kappa, E)$, κ dependences at $\kappa \rightarrow 0$ from calculated ones is mainly caused by the energetic inhomogeneity of $Sb(111)^{CE}$, $Sb(111)^{ECE}$, $Sb(001)^{CN}$ electrodes [1–4,8,23,24]. The fitting parameters established using random Gaussian roughness model (RGRM) are presented in Table 1. However, as for rough Cd and Bi electrodes [4,30], the experimental and theoretical roughness function values for rough $Sb(111)^{ECE}$, $Sb(111)^{CE}$ and $Sb(001)^{CN}$ surfaces are noticeably higher than the values established from AFM data.

6.4. *Ex situ* AFM measurements and roughness calculations of variously pre-treated Bi surfaces

According to the data of AFM studies on the surface of $Bi(111)^{CN}$ electrode, there are few thinly scattered break steps with height h_z from 0.4 to 1.5 nm, but the distance between these steps, l_x , is very large (up to 200 nm). At these flat regions of $Bi(111)^{CN}$, additionally some mono-atomic steps (with height from 0.25 to 0.35 nm) were found and the Rms values obtained using AFM method are very low ($R_{ms} \approx 0.36$ nm) (Table 1) [II]. The *ex situ* AFM data have been used for the calculation of the surface roughness factor values R_{AFM} and are given in Table 1. The results of theoretical simulation of this type of surface show that so prepared $Bi(111)^{CN}$ electrode is not very suitable for the experi-

mental verification of the new surface roughness theory [1–3] as the distance between the break steps is very large and R_{AFM} is very close to unity. According to the AFM studies of the surface of a cut at the room temperature $\text{Bi}(111)^C$ electrode shows mono-atomic or somewhat higher steps ($0.25 \div 0.70$ nm) ($R_{ms} = 0.44$ nm) and of small terraces with the medium lateral characteristic length (linear parameter) $l_x > 5$ nm. Theoretical simulation of $\text{Bi}(111)^C$ electrode surface shows very low surface roughness values (Table 1) like for $\text{Sb}(111)^C$ electrodes [I].

To prepare the surfaces with higher surface roughness, the $\text{Bi}(111)$ and $\text{Bi}(001)$ electrodes, cleaved at the room temperature, were additionally etched (during 3 sec. and 6 sec.) in the concentrated HNO_3 ($\text{Bi}(111)^{C1}$, $\text{Bi}(001)^{C1}$ and $\text{Bi}(001)^{C2}$, respectively). Fig. 17 (a) demonstrates the AFM image, histogram and surface height profile for the chemically etched $\text{Bi}(111)^{C1}$ whose surface has a more complicated structure in comparison with $\text{Bi}(111)^C$. The AFM images demonstrate the large surface pits with the medium linear parameter $l_x = 10 \dots 30$ μm and medium depth $0.4 \dots 1.1$ μm , and the smaller surface pits with the very different l_x and h_z values, as well as the pyramids with different height and width [II].

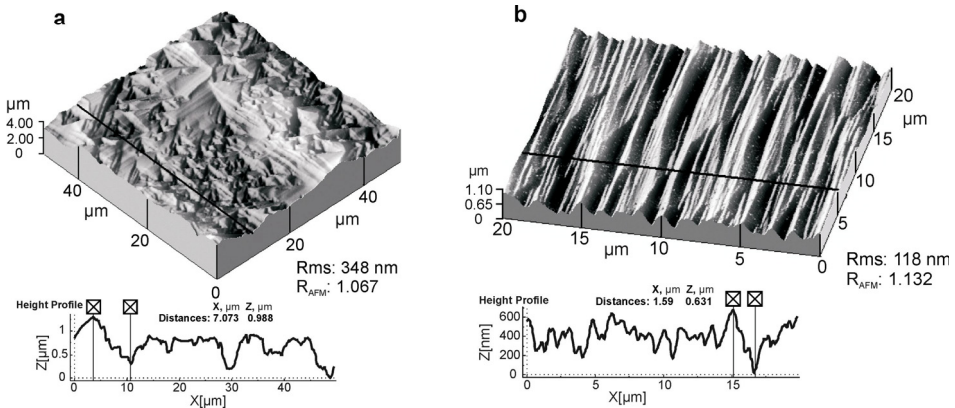


Fig. 17. AFM images and surface profiles for $\text{Bi}(111)^{CE}$ (a) and $\text{Bi}(001)^{C1}$ (cleaved and additionally chemically etched surface in HNO_3 during 3 sec.) (b) surfaces.

The AFM data of $\text{Bi}(001)^{C1}$ given in Fig. 17 (b) demonstrate the very complicated surface structure mainly in two directions (x , z). The comparatively high ridges and deep valleys with the medium height $h_z \leq 0.6$ μm and with the medium distance $l_x \sim 3.7$ μm between these valleys (surface profile in Fig. 17 (b)) have been established. However, on these big ridges, the less deeper furrows can be seen with the average distance of 10–100 nm and with the medium height 5–100 nm. Noticeably higher R_{ms} (118 nm) and R_{AFM} (1.13)

values (Table 1) have been established. On Bi(001)^{C2} surface, the more higher ridges (1.5...2.0 μm), R_{AFM} and R_{ms} values have been established (Table 1). It should be noted that, in the case of rough surfaces, the R_{ms} and R_{AFM} values noticeably depend on the region of surface area selected for analysis, and the values of R_{ms} and R_{AFM} noticeably decrease with the reduce of the surface area selected. However, for comparatively large surface area selected ($\geq 20 \times 20 \mu\text{m}$), the parameters obtained are practically independent of the selected region of the surface as well as of the surface area. Thus, the values of R_{ms} and R_{AFM} are very approximate quantities and probably only indicate the order of the increase of the surface roughness of the electrodes tested [4].

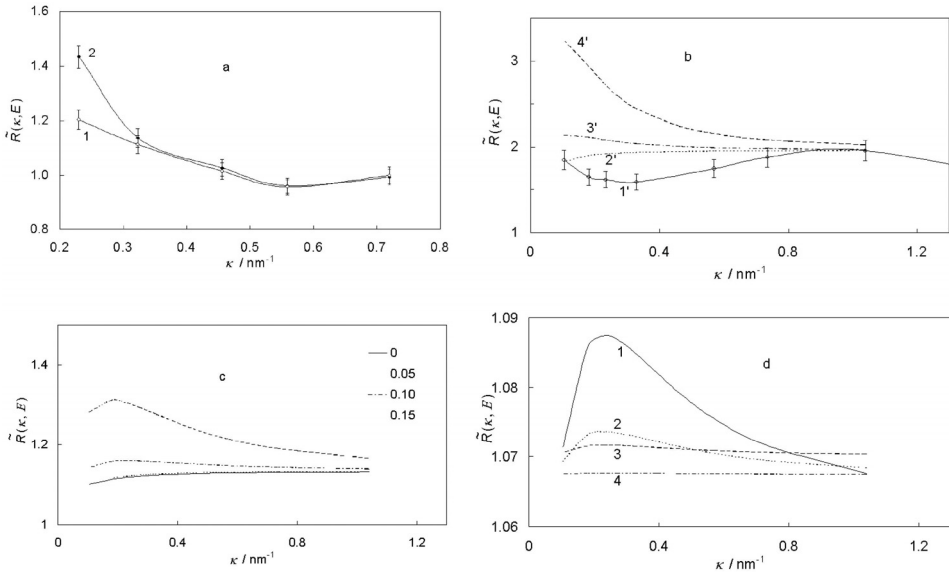


Fig. 18. Experimental (1;1';2) and theoretical (2';3';4'; calculated at $l_G = 3.0 \text{ nm}$ and $h = 0.5 \text{ nm}$) roughness function $\tilde{R}(\kappa, E)$ vs. inverse Debye length κ dependencies for Bi(001)^{C2} (a) and Bi(111)^{ECE} (b) in aqueous NaF solution at the fixed electrode rational potentials (V): 0 (1,1',2'); -0.1 (3'); -0.15 (4'); and -0.2 (2). $\tilde{R}(\kappa, E)$ vs. κ dependencies calculated according to the random Gaussian roughness model at the given $h = 5 \text{ nm}$ (root mean square height of surface roughness), $l_G = 10 \text{ nm}$ (characteristic lateral correlation length) at different rational electrode potentials, noted in figure (c); and for $E = -0.1 \text{ V}$ at $h = 2, l_G = 10$ (1); $h = 1, l_G = 10$ (2); $h = 0.5, l_G = 10$ (3); and $h = 0.2, l_G = 10$ (4).

The *ex situ* AFM data have been used for the calculation of the R_{AFM} values presented in Table 1 together with the data for electrochemically polished $\text{Bi}(111)^{EP}$ and electrochemically etched $\text{Bi}(111)^{ECE}$ [4]. According to the data in Table 1, R_{AFM} increases in the order of electrodes $\text{Bi}(111)^{EP} < \text{Bi}(111)^{CN} < \text{Bi}(111)^C < \text{Bi}(111)^{C1} < \text{Bi}(001)^{C1} < \text{Bi}(111)^{ECE} < \text{Bi}(001)^{C2}$ in a very good correlation with the root mean square roughness R_{ms} values [II].

Thus, to a first approximation, the random Gaussian roughness model (RGRM) (i.e. two-dimensional roughness model [1–3]) seems to be valid and, for that reason, mainly the theoretical surface roughness function values obtained according to RGRM have been calculated and discussed.

Fig. 18 (a and b) demonstrates the dependence of $\tilde{R}(\kappa, E)$ on the inverse Debye length (i.e. on the Gouy screening length), κ , of the electrolyte for various Bi electrodes. According to the systematized analysis of data it was found that if the rational potential decreases ($E \leq -0.1\text{V}$), the $\tilde{R}(\kappa, E), \kappa$ – curves become steeper (Fig. 18 (a)) in the range of $\kappa \leq 0.30 \text{ nm}^{-1}$, which is in a good agreement with the theoretical calculations (Fig. 18 (c and d)). At lower rational electrode potentials ($E < -0.1 \text{ V vs. } E_{\sigma=0}$), there has to be a maximum at $0.1 \text{ nm}^{-1} < \kappa \leq 0.3 \text{ nm}^{-1}$. At $\kappa \geq 0.5 \text{ nm}^{-1}$, the $\tilde{R}(\kappa, E)$ values level off to the so-called geometrical roughness factor R [1–3]. Therefore, for the fixed values of κ , the effect of surface structure on the differential capacitance values increases with the absolute value of the rational electrode potential in agreement with the theoretical calculations of Ref. [3] and our computer simulations (Fig. 18 (c and d)). According to the AFM data (Fig. 17) the medium distance between small consecutive peaks and valleys on the rough $\text{Bi}(001)^{C1}$ surface, l_x is on the order of 5 to 10 nm, thus the $\tilde{R}(\kappa, E), \kappa l_x$ – dependences have a weak maximum in the region $2 \leq \kappa l_x \leq 3.5$ in good agreement with the theoretical predictions of the new theory [1–3].

The results of theoretical calculations show that the $\tilde{R}(\kappa, E)$ values (at $\kappa = \text{const.}$) depend on the values of l_G and h , and increases with the ratio h/l_G (at $l_G = \text{const.}$) (Fig. 18 (d)) (l_G is the characteristic lateral correlation length and h is the root mean square height of surface roughness in RGRM). At $l_G = \text{const.}$ and $h/l_G = \text{const.}$ the value of $\tilde{R}(\kappa, E)$ increases with the absolute value of the rational electrode potential (Fig. 18 (c)) but the values of $\tilde{R}(\kappa, E)$ are practically independent of potential at $E \leq -0.3 \text{ V}$ [II].

7. CONCLUSIONS

The main aim of present work was to investigate some Bi and Sb electrode surfaces in *in situ* electrochemical condition to characterise the real surface structure by using scanning probe microscopy technique.

The *in situ* STM (scanning tunneling microscopy) studies of the Bi(111)^C (cleaved at the temperature of liquid nitrogen inside the glove box) and Bi(111)^{EP} (electrochemically polished) have been performed under negative polarisation in slightly acidified aqueous solutions.

The *in situ* atomic resolution for Bi(111)^C and Bi(111)^{EP} electrodes has been achieved [III,IV].

The *in situ* STM data show that the surface structure of Bi(111)^C and Bi(111)^{EP} have a very good stability within the wide potential region (−0.7 V to −0.1 V vs. Ag/AgCl (in saturated aqueous KCl solution)) in slightly acidified solutions and there are no quick surface reconstruction processes observed for Au(hkl) and discussed in the works [1–3,6]. Therefore it can be concluded that both Bi(111)^C and Bi(111)^{EP} electrodes can be used for the studies of the more complicated two-dimensional adsorption layers of various organic compounds at these surfaces [V].

The *in situ* STM studies on Sb(111)^{EP} electrode surface show some atomically flat areas. The atomic resolution in the 5×10^{-2} M Na₂SO₄ + 3.12×10^{-5} M H₂SO₄ aqueous solution for Sb(111)^{EP} electrode has been achieved.

The UHV-STM (ultra high vacuum scanning tunneling microscopy) study indicates that the surface of Sb(111)^{CN} (cleaved at the temperature of liquid nitrogen) is very inactive and chemically stable in air as well as in the conditions of reduced pressure during many hours. The atomic resolution has been achieved without any additional treatment of Sb(111)^{CN} surface in UHV [I].

Impedance spectroscopy and *in situ* STM have been used for investigation of the camphor adsorption at the electrochemically polished Bi(111) electrode from weakly acidified Na₂SO₄ aqueous base electrolyte solution [V]. The influence of the electrode potential on the adsorption kinetics and camphor layer structure at Bi(111) has been demonstrated. It was found that the stable adsorbate adlayer (2D condensation) detectable by using the *in situ* STM method has been observed only at the positively charged electrode surface, where the weak co-adsorption of SO₄²⁻ anions and camphor molecules is possible [V].

A new Debye length dependent surface roughness model, based on the non-linear Poisson — Boltzmann theory, developed by Daikhin, Kornyshev and Urbakh [1–3], has been used for interpretation of the experimental AFM (atomic force microscopy) and impedance (capacitance) data of variously pre-treated Bi and Sb electrodes. It was found that the different roughness parameters (Rms (root mean square roughness), R_{AFM} (geometrical roughness factor), f_{p-z} , (Parsons — Zobel roughness coefficient) and $\tilde{R}(\kappa, \sigma = 0)$

(roughness function at surface charge density $\sigma = 0$) calculated using models discussed in the works [I,II], have comparable values for the geometrically flat and energetically homogeneous surfaces studied but it increases in the same order for other surfaces studied. For Bi electrodes the roughness increases in the order $\text{Bi}(111)^{\text{EP}} < \text{Bi}(111)^{\text{CN}} < \text{Bi}(111)^{\text{C}} < \text{Bi}(111)^{\text{ECE}} < \text{Bi}(001)^{\text{C1}} < \text{Bi}(111)^{\text{C1}} < \text{Bi}(001)^{\text{C2}}$ [II] and for Sb electrodes in the order: $\text{Sb}(111)^{\text{CN}} < \text{Sb}(111)^{\text{EP}} < \text{Sb}(111)^{\text{ECE}} < \text{Sb}(111)^{\text{CE}} < \text{Sb}(001)^{\text{CN}}$ [I].

However, it is demonstrated that the new Debye length dependent surface roughness model overestimates the surface roughness values for the geometrically rough surfaces and the future corrections, taking into account the influence of energetic inhomogeneity of the polycrystalline surfaces (i.e. the non-equal surface charge density values at the various homogeneous regions exposed at the macro-polycrystalline electrode surface) on the interfacial capacitance and local charge density values, are inevitable.

8. REFERENCES

- [1] L. I. Daikhin, A. A. Kornyshev and M. Urbakh, *Phys. Rev. E* 53 (1996) 6192.
- [2] L. I. Daikhin, A. A. Kornyshev and M. Urbakh, *Electrochim. Acta* 42 (1997) 2853.
- [3] L. I. Daikhin, A. A. Kornyshev and M. Urbakh, *J. Chem. Phys.* 108 (1998) 1715.
- [4] E. Lust, A. Jänes, V. Sammelselg, P. Miidla and K. Lust, *Electrochim. Acta* 43 (1998) 373.
- [5] A. Hamelin, in J. O'M. Bockris, B.E. Conway and R. E. White (eds.), *Modern Aspects of Electrochemistry*, Vol. 16, Plenum, New York, 1985, p.1.
- [6] D. M. Kolb, *Ber. Bunsenges Phys. Chem.* 92 (1988) 1175.
- [7] D. M. Kolb, in J. Lipkowski and P.N. Ross (Eds.) *Structure of Electrified Interfaces*, VCH, New York, 1993, p. 65.
- [8] M. A. Vorotyntsev, in J. O'M. Bockris, B. E. Conway and R. E. White (eds.), *Modern Aspects of Electrochemistry*, Vol. 17, Plenum, New York, 1986, p.131.
- [9] N. A. Paltusova, A. R. Alumaa, U. V. Palm, *Elektrokhimiya* 16 (1980) 1249.
- [10] H. Steigler, D. Krznarić, D. M. Kolb, *J. Electroanal. Chem.* 532 (2002) 227.
- [11] W. Schmickler, *Chem. Rev.* 96 (1996) 3177.
- [12] A. Vaught, T. W. Jing, S. M. Lindsay, *Chem. Phys. Lett.* 236 (1995) 306.
- [13] W. Schmickler, D. Henderson, *J. Electroanal. Chem* 290 (1990) 283.
- [14] C. J. Chen, *Introduction to Scanning Tunneling Microscopy*, Oxford University Press, New York, 1993.
- [15] D. M. Eigler, P. S. Weiss, E. K. Schweizer et al., *Phys. Rev. Lett.* 66 (1991) 1189.
- [16] W. Schmickler, *J. Electroanal. Chem.* 296 (1990) 283.
- [17] P. Sautet, *Chem. Rev.* 97 (1997) 1097.
- [18] P. Sautet, *Surf. Sci.* 374 (1997) 406.
- [19] A. J. Bard, F. F. Fan, J. Kwak and O. Lev, *Anal. Chem.* 61 (1989) 132.
- [20] J. Lipkowski, P. N. Ross, (Eds.), *Imaging of Surfaces and Interfaces*, Wiley-VCH, New York, 1999.
- [21] H. Siegenthaler, *STM in Electrochemistry in Scanning Tunneling Microscopy II* (Eds.: R. Wiesendanger, H. J. Gunterodt), Springer-Verlag, New York, 1992.
- [22] T. P. Moffat, in A. J. Bard, M. Stratman (Eds.), *Encyclopedia of Electrochemistry*, Vol. 3, Wiley-VCH, Weinheim, 2002, p. 393.
- [23] M. P. Soriaga, D. A. Harrington, J. L. Stikney, A. Wieckowski, in R. E. White, J. O'M. Bockris and B. E. Conway (Eds.), *Modern Aspects of Electrochemistry*, vol. 28, Plenum, New York, 1996, p. 1.
- [24] S. Trasatti and E. Lust, in R. E. White, J. O'M. Bockris and B. E. Conway (Eds.), *Modern Aspects of Electrochemistry*, V. 33, Kluwer Academic / Plenum Publishers, New York, 1999, p. 1.
- [25] A. Hamelin and P. Dechy, *Compt. Rend., Ser. C* 276 (1973) 33.
- [26] A. Hamelin, L. Stoicoviciu, *J. Electroanal. Chem.* 236 (1987) 267.
- [27] X. Gao, G. J. Edens, A. Hamelin, M. J. Weaver, *Surf. Sci.* 296 (1993) 333.
- [28] D. M. Kolb and J. Schneider, *Surf. Sci.* 162 (1985) 764.
- [29] D. M. Kolb, J. Schneider, *Electrochim. Acta* 31 (1986) 929.
- [30] G. Valette and A. Hamelin, *J. Electroanal. Chem.* 45 (1973) 301.
- [31] A. Hamelin, L. Stoicoviciu, *J. Electroanal. Chem.* 271 (1989) 15.
- [32] J. Clavilier, R. Taure, G. Guinet, *J. Electroanal. Chem.* 107 (1980) 205.

- [33] M. Höpfner, W. Obretenov, K. Jüttner, W. J. Lorenz, G. Staikov, V. Bostanov, E. Budevski, *Surf. Sci.* 248 (1991) 225.
- [34] W. Obretenov, M. Höpfner, W. J. Lorenz, E. Budevski, G. Staikov, H. Siegenthaler, *Surf. Sci.* 271 (1992) 191.
- [35] J. W. Mathews (Ed.), *Epitaxial Growth*, Vol. A and B, Academic Press, New York, 1975.
- [36] N. Batina, A. S. Dakkouri, D. M. Kolb, *J. Electroanal. Chem.* 370 (1984) 87.
- [37] G. L. Borges, M. G. Samant, K. Ashely, *J. Electrochem. Soc.* 139 (1992) 1565.
- [38] R. Gomez, M. J. Weaver, *J. Electroanal. Chem.* 435 (1997) 205.
- [39] Th. Wandlowski, A. J. Bard, M. Stratman (Eds) *Encyclopedia of Electrochemistry* Vol. 1. Wiley-VCH, Weinheim, 2002, p. 383.
- [40] D. M. Kolb, *Prog. Surf. Sci.* 51 (1996), 109.
- [41] R. Sonnenfeld, J. Schneir, P. K. Hansma, in R. E. White, J. O'M. Bockris and B. E. Conway (Eds.), *Modern Aspects of Electrochemistry*, vol. 21, Plenum, New York, 1996, p. 1.
- [42] W. B. Pearson, *The Crystal Chemistry and Physics of Metals and Alloys*, Wiley-Interscience, 1972), p. 280.
- [43] M. Roberts, C. Makky, *Khimiya poverhnosty razdela metall-gaz*, Moscow, 1981.
- [44] E. Lust, K. Lust and A. Jänes, *Russian. J. Electrochem.* 31 (1995) 807.
- [45] E. Lust, A. Jänes, V. Sammelselg, P. Miidla, *Electrochim. Acta*, 46 (2000) 185.
- [46] D. Mayer, Th. Dretschov, K. Ataka, Th. Wandlowski, *J. Electroanal. Chem.* 524–525 (2002) 20.
- [47] Th. Dreschkov, Th. Wandlowski, *Electrochim. Acta* 45 (1999) 731.
- [48] Th. Dreschkov, D. Lampner, Th. Wandlowski, *J. Electroanal. Chem.* 458 (1999) 121.
- [49] Q. Jin, J. A. Rodriguez, C. Z. Li, Y. Darici, N. J. Tao, *Surf. Sci.* 425 (1999) 101.
- [50] I. Burgess, C. A. Jeffrey, X. Cai, G. Szymanski, Z. Galus, J. Lipkowski, *Langmuir* 15 (1999) 2607.
- [51] P. Müller, A. Ando, T. Yamada, K. Itoya, *J. Electroanal. Chem.* 467 (1999) 282.
- [52] V. Maurice, L. H. Klein, H-H. Strehblow, P. Marcus, *J. Electrochem. Soc.*, 150 (7) B316–B324.
- [53] K. G. Baikerikar, S. Sathyanaranayana, *J. Electroanal. Chem.* 24 (1970) 333.
- [54] C. Buess-Herman, C. Frank, L. Gierst, *Electroanal. Chem.* 329 (1992) 91.
- [55] S. Sridharan, R. de Levie, *J. Electroanal. Chem.* 205 (1986) 303.
- [56] S. L. Dyatkina, B. B. Damaskin, N. V. Fedorovich, E. V. Stenina, V. A. Yusupova, *Elektrokhimiya* 9 (1978) 1283.
- [57] N. A. Paltusova, A. R. Alumaa, U. V. Palm, *Elektrokhimiya* 15 (1979) 1723.
- [58] A. N. Frumkin, *Potentsialy nulevogo zaryada (Potentials of zero charge)*, Nauka, Moscow, 1979.
- [59] J. Clavilier, *J. Electroanal. Chem.* 107 (1980) 211.
- [60] S. Trasatti and O.A. Petrii, *Pure Appl. Chem.* 67 (1991) 711.
- [61] R. C. Salvarezza and A. J. Ariva, in *Modern Aspects of Electrochemistry*, Vol. 28, J. O'M. Bockris, B. E. Conway and R. E. White, Editors, Plenum, New York, 1995, p. 289.
- [62] U. V. Palm, M. P. Pärnoja and N. B. Grigoryev, *Elektrokhimiya*, 13 (1977) 1074.
- [63] R. Parsons and F. R. G. Zobel, *J. Electroanal. Chem.*, 9 (1965) 333.
- [64] I. A. Bagotskaya, M. D. Levi and B. B. Damaskin, *J. Electroanal. Chem.*, 115 (1980) 189.

- [65] M. A. Vorotyntsev, *J. Electroanal. Chem.*, 123 (1981) 379.
- [66] A. J. Bard, *Anal. Chem.*, 33 (1961) 11.
- [67] A. Hamelin, T. Vitanov, E. Sevastyanov and A. Popov, *J. Electroanal. Chem.*, 145 (1983) 225.
- [68] G. Stoikov, E. Budevski, W. Obretenov and W. Lorenz, *J. Electroanal. Chem.*, 349 (1993) 355.
- [69] X. Gao, A. Hamelin and M.W. Weaver, *Phys. Rev. Lett.*, 67 (1991) 616.
- [70] M. Urbakh and L. Daikhin, *Phys. Rev. B*, 49 (1994) 4866.
- [71] M. A. Vorotyntsev, in *Itogi nauki i tekhniki. Elektrokimiya*, Vol 21, Yu. M. Polukarov, Editor, Nauka, Moscow, 1984, p. 3.
- [72] E. Lust, K. Lust and A. Jänes, *J. Electroanal. Chem.*, 413 (1996) 111.
- [73] E. Lust, A. Jänes, K. Lust, V. Sammelselg and P. Miidla, *Electrochimica Acta*, 42 (1997) 2861.
- [74] G. Jarzabek, Z. Borkowska, *Electrochim. Acta*, 42 (1997) 2915.
- [75] A. Tymosiak-Zielinska and Z. Borkowska, *Electrochim. Acta*, 45 (2000) 3105.
- [76] E. J. Lust, A. J. Janes, K. K. Lust, J. J. Ehrlich, *Rus. J. Electrochem.*, 32 (1996) 943.
- [77] E. Lust, A. Jänes, K. Lust, M. Väärtnõu, *Electrochim. Acta*, 42 (1997) 771.
- [78] A. Kelli, G. W. Crowes, *Crystallography and Crystal Defects*, Longman, London, 1970, p. 129.
- [79] G. Nurk, A. Jänes, K. Lust, E. Lust, *J. Electroanal. Chem.* 515 (2001) 17.
- [80] H. Kasuk, G. Nurk, K. Lust, E. Lust, *J. Electroanal. Chem.* 550–551 (2003) 13.
- [81] A. Lasia, in: B. E. Conway, J. O'M. Bockris (Eds.), *Modern Aspects of Electrochem.*, Vol. 32, Plenum Press, New York, 1999, p. 143.
- [82] E. J. Lust, U. V. Palm, *Soviet Electrochem. Engl. Tr.* 24 (1988) 227.
- [83] E. Lust, U. Palm, *Elektrokimiya* 21 (1985) 1304.
- [84] H. K. Roobottom, H. B. Jenkins, J. Passmore, L. Glasser, *J. Chem. Ed.* 76 (1999) 1570.
- [85] C. Triot, *Curves and Fractal Dimensions*, Springer, Berlin, 1995.
- [86] A. A. Kornyshev, J. Ulstrup, *Chem. Scr.* 25 (1985) 58.
- [87] A. A. Kornyshev, W. Schmickler, M. A. Vorotyntsev, *Phys. Rev. B* 25 (1982) 771.

9. SUMMARY IN ESTONIAN

Pinnastruktuur erinevate vismuti ja antimoni monokristalliliste elektrootide korral

Käesoleva töö eesmärk oli välja selgitada erinevate Bi ja Sb elektrootide pinnastruktuur reaalsetes elektrokeemilistes süsteemides kasutades selleks erinevaid skaneeriva teravikmikroskoopia võimalusi.

Töö teostamise käigus töötati välja Bi ja Sb elektrootide uuringuteks sobivad tehnilised lahendused kõrge lahutusvõimega *in situ* STM uuringute läbiviimiseks erinevate elektrolüütide lahustes.

Vedela lämmastiku temperatuuril lõhestatud ja elektrokeemiliselt poleeritud Bi(111) elektrootidel saavutati atomaarne lahutus [III,IV]. Samuti kinnitavad tulemused, et erinevalt prepareeritud Bi(111) elektrootide regulaarne pinnastruktuur on väga stabiilne laias potentsiaalide vahemikus (–0.7 V kuni –0.1 V vs. Ag/AgCl (küllastatud KCl lahuses)) nõrgalt happelistes elektrolüütides ning seal ei esine kiireid pinna rekonstrueerumise protsesse, mida on laialdaselt täheldatud erinevatel kulla monokristalli tahkudel [1–3,6]. Seetõttu võib järeldada, et lõhestatud ja elektrokeemiliselt poleeritud Bi(111) elektrootid sobivad mudelpinnana väga hästi erinevate orgaaniliste ühendite komplitseeritud kahe-dimensionaalsete adsorbeerunud monokihtide uuringuteks, kuna võimaldavad välistada aluspinna pinddifusioonist põhjustatud moonutusi [V].

Sarnaselt Bi põhitalule on saavutatud nõrgalt hapestatud elektrolüüdis *in situ* atomaarne lahutus ka elektrokeemiliselt poleeritud Sb(111) elektrootil.

Ülikõrgvaakumis teostatud STM uuringud vedela lämmastiku keemise temperatuuril lõhestatud Sb(111) tahule kinnitavad selle inaktiivsust ja keemilist stabiilsust nii lühiajalisel õhukeskkonnas viibimisel kui ka vaakumi tingimustes. On märkimisväärne, et lõhestatud antimoni põhitalul osutus atomaarse lahutuse saavutamise võimalikuks ilma tavapärase täiendava elektrooti pinna töötluseta (kuumutamine, Ar⁺-pommitamine jne) kõrgvaakumi tingimustes [I].

In situ STM meetodil õnnestus detekteerida ja visualiseerida kahedimensionaalse adsorbeerunud kampri monokihi struktuur elektrokeemiliselt poleeritud Bi(111) elektrooti pinnal nõrgalt hapestatud Na₂SO₄ vesilahuses [V]. Samuti demonstreeriti elektrooti potentsiaali mõju kampri monokihi moodustumise kineetikale. Leiti, et *in situ* STM meetodi jaoks on kampri adsorbeerunud monokiht detekteeritav vaid elektrooti positiivsemate pinnalaengute korral, mis võib viidata spetsiifiliselt adsorbeerunud SO₄²⁻ ionide osalusele adsorptsioonikihi moodustumisel [V].

Erinevalt prepareeritud Bi ja Sb elektrootide pinnakareduse modelleerimiseks ja eksperimentaalsete AFM ja impedantspektroskoopia (diferentsiaal-mahtuvuse) andmete interpreteerimiseks kasutati Daikhini, Kornyshevi ja Urbakhi poolt välja töötatud uut Debye ekraneerimispikkust arvestavat ja Poisson-Boltzmanni teoorial põhinevat pinnakareduse mudelit [1–3]. Leiti, et

erinevalt leitud karedusfaktorid (R_{rms} (ruutkeskmine hälve keskmisest pinnakonaruse kõrgusest), R_{AFM} (geomeetriline karedusfaktor), $f_{\text{p-z}}$ (Parzons — Zobeli karedusfaktor) ja $\tilde{R}(\kappa, \sigma = 0)$ (karedusfunktsioon pinna laengu tiheduse $\sigma = 0$ juures)) annavad kokkulangevaid tulemusi geomeetriliselt suhteliselt siledade ja energeetiliselt homogeenemate pindade korral, kuid muutuvad samas järjekorras ka teiste uuritud pindade korral. Uuritud Bi elektrodide korral suureneb pinnakaredus järjekorras: $\text{Bi}(111)^{\text{EP}} < \text{Bi}(111)^{\text{CN}} < \text{Bi}(111)^{\text{C}} < \text{Bi}(111)^{\text{ECE}} < \text{Bi}(001)^{\text{C1}} < \text{Bi}(111)^{\text{C1}} < \text{Bi}(001)^{\text{C2}}$ [II] ja uuritud Sb elektrodide korral: $\text{Sb}(111)^{\text{CN}} < \text{Sb}(111)^{\text{EP}} < \text{Sb}(111)^{\text{ECE}} < \text{Sb}(111)^{\text{CE}} < \text{Sb}(001)^{\text{CN}}$ [I].

Leiti, et Debye ekraneerimispikkust arvestav uus karedusmudel ülehindab geomeetriliselt karedamate elektrodide pinnakaredust ja vajab seega täiustamist arvestamiseks pinna energeetilise ebahütluse mõju ning pinnalaengu tiheduse fluktuatsioone pinna eri osadel.

10. ACKNOWLEDGEMENTS

The present study was performed at the Institute of Physical Chemistry of the University of Tartu. The support received from Estonian Science Foundation (grants 4568, 5032, 5803 and 6455).

First and foremost I would like to express my gratitude to my supervisor Professor Enn Lust for persistent assistance and scientific guidance through the years of our collaboration.

I am very thankful to Professor Väino Sammelselg, who introduced me to the Scanning Probe Microscopy and has been my initial advisor.

I am also very thankful to Professor Juhani Väyrynen for collaboration and for the opportunity to work in his laboratory at the University of Turku.

Dr. Alar Jänes and Assoc. Prof. Peep Miidla are specially acknowledged for collaboration in roughness calculations and computer simulations.

I would like to thank all my friends and colleagues for helpful discussions, inspiration and continuous support.

I deeply appreciate the unfailing support of my family during all these years.

11. PUBLICATIONS

CURRICULUM VITAE

Silvar Kallip

Born: October 28, 1978, Rakvere, Estonia
Citizenship: Estonian
Marital status: single
Address: University of Tartu, Institute of Physical Chemistry
2 Jakobi St. 51014 Tartu, Estonia
Phone: +372 737 5163
Fax: +372 737 5160
e-mail: silvar.kallip@ut.ee

Education

1996–2000 University of Tartu, Department of Chemistry, *B.Sc.*
(chemistry) 2000
2000–2002 University of Tartu, Department of Chemistry, *M.Sc.*
(chemistry) 2002
2002–present University of Tartu, Department of Chemistry, *Ph.D.* student,
doctoral advisor prof. Enn Lust

Professional employment and retraining

2000 University of Tartu, Institute of Physics, laboratory assistant
2000–2002 University of Tartu, Institute of Physical Chemistry, chemist
2003–2004 University of Tartu, Institute of Physical Chemistry, temporary
researcher
2004–present University of Tartu, Institute of Physical Chemistry, researcher

Major scientific publications

1. E. Lust, S. Kallip, P. Möller, A. Jänes, V. Sammelselg, P. Miidla, M. Väärtnõu and K. Lust, Influence of surface charge density on the electrochemically derived surface roughness of Bi electrodes, *J. Electrochem. Soc.* 150 (2003) E175–E184.
2. S. Kallip, P. Laukkanen, A. Jänes, V. Sammelselg, J. Väyrynen, P. Miidla, E. Lust, Investigation of the surface topography and double layer charac-

- teristics of variously pre-treated antimony single crystal electrodes, *Surf. Sci.* 532–535 (2003) 1121–1126.
3. E. Lust, G. Nurk, A. Jänes, M. Arulepp, P. Nigu, L. Permann, P. Möller, S. Kallip, V. Sammelselg, Electrochemical properties of nanoporous carbon electrodes in various nonaqueous electrolytes, *J. Solid State Electrochem.* 7 (2003) 91–105
 4. E. Lust, G. Nurk, P. Möller, I. Kivi, S. Kallip, A. Janes, V. Sammelselg, H. Mändar, Electrochemical Impedance Characteristics of Some Medium Temperature Semicells for SOFC, *Proc. of the Internat. Symp. on Solid Oxide Fuel Cells*, Paris, France, 2003, 1176–1185.
 5. G. Nurk, S. Kallip, I. Kivi, P. Möler, E. Lust, Electrochemical Characteristics of $Ce_{1-x}Gd_xO_{2-\delta} | La_{1-x}Sr_xCoO_{3-\delta} + Ce_{1-x}Gd_xO_{2-\delta}$ Half-Cell, Sixth European Solid Oxide Fuel Cell Forum, Lucerne, Switzerland (2004) 887–896.
 6. E. Lust, G. Nurk, S. Kallip, I. Kivi, P. Möller, P. Nigu, K. Lust, Systematic Analysis of Some Medium Temperature Half-Cells for SOFC, Sixth European Solid Oxide Fuel Cell Forum, Lucerne, Switzerland (2004) 1271–1280.
 7. S.Kallip, E. Lust, In situ STM studies of Bi(111) electrodes in aqueous electrolyte solutions, *Electrochem. Comm.* 7 (2005) 863–867.
 8. E. Lust, P. Möller, I. Kivi, G. Nurk, S. Kallip, P. Nigu, K. Lust, Optimisation of the cathode composition for the intermediate temperature SOFC, *Proc. of 9th Internat. Symp. on Solid Oxide Fuel Cells*, Quebec (2005) 1607–1616.
 9. E. Lust, G. Nurk, S. Kallip, I. Kivi, P. Möller, Electrochemical characteristics of $Ce_{0.8}Gd_{0.2}O_{1.9} | La_{0.6}Sr_{0.4}CoO_{3-\delta} + Ce_{0.8}Gd_{0.2}O_{1.9}$ half-cell, *J. Solid State Electrochem* 9 (2005) 674–683.
 10. E. Lust, P. Möller, I. Kivi, G. Nurk, S. Kallip, Electrochemical characteristics of $La_{0.6}Sr_{0.4}CoO_{3-\delta}$, $Pr_{0.6}Sr_{0.4}CoO_{3-\delta}$ and $Gd_{0.6}Sr_{0.4}CoO_{3-\delta}$ on $Ce_{0.85}Sm_{0.15}O_{1.925}$ electrolyte, *J. Solid State Electrochem* 9 (2005) 882–889.
 11. Enn Lust, Priit Möller, Indrek Kivi, Gunnar Nurk, Silvar Kallip, Priit Nigu, Karmen Lust, Optimisation of the cathode composition for the intermediate temperature SOFC, *J. Electrochem. Soc.* 152 (2005) A2306–A2308.
 12. E. Lust, G. Nurk, P. Möller, I. Kivi, S. Kallip, Oxygen reduction and electrochemical characteristics of half-cells for intermediate SOFCs, 26th Risø International Symposium on Materials Science, Risø, (2005) 279–284.
 13. E. Lust, J. Nerut, E. Härk, S. Kallip, V. Grozovski, T. Thomberg, R. Jäger, K. Lust, K. Tähnas Electroreduction of Complex Ions at Bismuth and Cadmium Single Crystal Plane Electrodes”, *Electrochem. Soc. Trans.* (2006), Vol. 1, “Molecular Structure Effects in Heterogeneous Electron Transfer Kinetics”, (accepted).
 14. P. Möller, G. Nurk, I. Kivi, S. Kallip, E. Lust, Influence of electrode potential on the oxygen reduction kinetics on the intermediate temperature SOFCs cathodes, *Solid State Ionics* (submitted).
 15. S. Kallip, H. Kasuk, V. Grozovski, E. Lust, Adsorption of camphor at Bi(111) electrode, *Electrochem. Comm.* (submitted).

ELULOOKIRJELDUS

Silvar Kallip

Sündinud: 28. oktoober 1978, Rakvere, Eesti Vabariik
Kodakondsus: Eesti
Perekonnaseis: vallaline
Aadress: Tartu Ülikool, Füüsikalise keemia instituut
Jakobi 2, 51014 Tartu, Eesti
Tel: +372 737 5163
Fax: +372 737 5160
e-mail: silvar.kallip@ut.ee

Haridus

1996–2000 Tartu Ülikooli keemiaosakonna üliõpilane, *B.Sc.* (keemia) 2000
2000–2002 Tartu Ülikooli keemiaosakonna magistrant, *M.Sc.* (keemia) 2002
2002– Tartu Ülikooli keemiaosakonna doktorant, juhendaja prof.
Enn Lust

Teenistuskäik

2000 Tartu Ülikool, Füüsika instituut, laborant
2001–2002 Tartu Ülikool, Füüsikalise keemia instituut, keemik
2003–2004 Tartu Ülikool, Füüsikalise keemia instituut, erakorraline teadur
2004– Tartu Ülikool, Füüsikalise keemia instituut, teadur

Olulisemad publikatsioonid

1. E. Lust, S. Kallip, P. Möller, A. Jänes, V. Sammelselg, P. Miidla, M. Väärtnõu and K. Lust, Influence of surface charge density on the electrochemically derived surface roughness of Bi electrodes, *J. Electrochem. Soc.* 150 (2003) E175–E184.
2. S. Kallip, P. Laukkanen, A. Jänes, V. Sammelselg, J. Väyrynen, P. Miidla, E. Lust, Investigation of the surface topography and double layer characteristics of variously pre-treated antimony single crystal electrodes, *Surf. Sci.* 532–535 (2003) 1121–1126.
3. E. Lust, G. Nurk, A. Jänes, M. Arulepp, P. Nigu, L. Permann, P. Möller, S. Kallip, V. Sammelselg, Electrochemical properties of nanoporous carbon electrodes in various nonaqueous electrolytes, *J. Solid State Electrochem.* 7 (2003) 91–105

4. E. Lust, G. Nurk, P. Möller, I. Kivi, S. Kallip, A. Janes, V. Sammelselg, H. Mändar, Electrochemical Impedance Characteristics of Some Medium Temperature Semicells for SOFC, Proc. of the Internat. Symp. on Solid Oxide Fuel Cells, Paris, France, 2003, 1176–1185.
5. G. Nurk, S. Kallip, I. Kivi, P. Möler, E. Lust, Electrochemical Characteristics of $Ce_{1-x}Gd_xO_{2-\delta} | La_{1-x}Sr_xCoO_{3-\delta} + Ce_{1-x}Gd_xO_{2-\delta}$ Half-Cell, Sixth European Solid Oxide Fuel Cell Forum, Lucerne, Switzerland (2004) 887–896.
6. E. Lust, G. Nurk, S. Kallip, I. Kivi, P. Möller, P. Nigu, K. Lust, Systematic Analysis of Some Medium Temperature Half-Cells for SOFC, Sixth European Solid Oxide Fuel Cell Forum, Lucerne, Switzerland (2004) 1271–1280.
7. S.Kallip, E. Lust, In situ STM studies of Bi(111) electrodes in aqueous electrolyte solutions, *Electrochem. Comm.* 7 (2005) 863–867.
8. E. Lust, P. Möller, I. Kivi, G. Nurk, S. Kallip, P. Nigu, K. Lust, Optimisation of the cathode composition for the intermediate temperature SOFC, Proc. of 9th Internat. Symp. on Solid Oxide Fuel Cells, Quebec (2005) 1607–1616.
9. E. Lust, G. Nurk, S. Kallip, I. Kivi, P. Möller, Electrochemical characteristics of $Ce_{0.8}Gd_{0.2}O_{1.9} | La_{0.6}Sr_{0.4}CoO_{3-\delta} + Ce_{0.8}Gd_{0.2}O_{1.9}$ half-cell, *J. Solid State Electrochem* 9 (2005) 674–683.
10. E. Lust, P. Möller, I. Kivi, G. Nurk, S. Kallip, Electrochemical characteristics of $La_{0.6}Sr_{0.4}CoO_{3-\delta}$, $Pr_{0.6}Sr_{0.4}CoO_{3-\delta}$ and $Gd_{0.6}Sr_{0.4}CoO_{3-\delta}$ on $Ce_{0.85}Sm_{0.15}O_{1.925}$ electrolyte, *J. Solid State Electrochem* 9 (2005) 882–889.
11. Enn Lust, Priit Möller, Indrek Kivi, Gunnar Nurk, Silvar Kallip, Priit Nigu, Karmen Lust, Optimisation of the cathode composition for the intermediate temperature SOFC, *J. Electrochem. Soc.* 152 (2005) A2306–A2308.
12. E. Lust, G. Nurk, P. Möller, I. Kivi, S. Kallip, Oxygen reduction and electrochemical characteristics of half-cells for intermediate SOFCs, 26th Risø International Symposium on Materials Science, Risø, (2005) 279–284.
13. E. Lust, J. Nerut, E. Härk, S. Kallip, V. Grozovski, T. Thomberg, R. Jäger, K. Lust, K. Tähnas Electroreduction of Complex Ions at Bismuth and Cadmium Single Crystal Plane Electrodes”, *Electrochem. Soc. Trans.* (2006), Vol. 1, “Molecular Structure Effects in Heterogeneous Electron Transfer Kinetics”, (accepted).
14. P. Möller, G. Nurk, I. Kivi, S. Kallip, E. Lust, Influence of electrode potential on the oxygen reduction kinetics on the intermediate temperature SOFCs cathodes, *Solid State Ionics* (submitted).
15. S. Kallip, H. Kasuk, V. Grozovski, E. Lust, Adsorption of camphor at Bi(111) electrode, *Electrochem. Comm.* (submitted).